DYNAMIC MAPPING OF HUMAN BRAIN FUNCTION AND BEHAVIOR

by

Michael Adam Ferguson

A dissertation submitted to the faculty of
The University of Utah
in partial fulfillment of requirements for the degree of

Doctor of Philosophy

Department of Bioengineering

The University of Utah

August 2016

The University of Utah Graduate School

STATEMENT OF DISSERTATION APPROVAL

The dissertation of **Michael Adam Ferguson**

has been approved by the following supervisory committee members:

Jeffrey S. Anderson	, Chair	**07/13/2015** Date Approved
Orly Alter	, Member	**07/13/2015** Date Approved
Guido Gerig	, Member	**07/13/2015** Date Approved
Thomas Fletcher	, Member	Date Approved
Edward W. Hsu	, Member	Date Approved

and by **Robert Hitchcock** , Chair/Dean of the Department/College/School of **Bioengineering**

and by David B. Kieda, Dean of The Graduate School.

ABSTRACT

The human brain is the seat of cognition and behavior. Understanding the brain mechanistically is essential for appreciating its linkages with cognitive processes and behavioral outcomes in humans. Mechanisms of brain function categorically represent rich and widely under-investigated biological substrates for neural-driven studies of psychiatry and mental health. Research examining intrinsic connectivity patterns across whole brain systems utilizes functional magnetic resonance imaging (fMRI) to trace spontaneous fluctuations in blood oxygen-level dependent (BOLD) signals. In the first study presented, we reveal patterns of dynamic attractors in resting state functional connectivity data corresponding to well-documented biological networks. We introduce a novel simulation for whole brain dynamics that can be adapted to either group-level analysis or single-subject level models. We describe stability of intrinsic functional architecture in terms of transient and global steady states resembling biological networks. In the second study, we demonstrate plasticity in functional connectivity following a minimum six-week intervention to train cognitive performance in a speed reading task. Long-term modulation of connectivity with language regions indicate functional connectivity as a candidate biomarker for tracking and measuring functional changes in neural systems as outcomes of cognitive training. The third study demonstrates utility of functional biomarkers in

predicting individual differences in behavioral and cognitive features. We successfully predict three major domains of personality psychology—intelligence, agreeableness, and conscientiousness—in individual subjects using a large (N=475) open source data sample compiled by the National Institutes of Health's Human Connectome Project.

TABLE OF CONTENTS

LIST OF FIGURES

ACKNOWLEDGEMENTS

I would like to thank my committee members for their guidance and insight. Their belief in my abilities and support for my interests have been indispensable gifts. Profound thanks are owed to my committee chair, Dr. Jeffrey S. Anderson, for his masterful skill, mentoring, patience, and vision. He is a teacher and a friend.

I am grateful to my parents for their ongoing pride in my education and research. I express loving thanks to my devoted John Seth Anderson, husband and partner in the life of the mind.

Research icons of history have provided motivation and ambition to me, time and time again. I give special acknowledgements to the lives and legacies of Alan Turing and William James for their inspiration in my craft.

MRI scanning costs were funded by the Flamm Family Foundation and Morrell Family Foundation. Jeff Flamm is CEO of EyeQ Advantage, which provided the software used in cognitive training free of charge for the study. The study authors have no financial interest in the EyeQ software or EyeQ Advantage company.

Data were provided by the Human Connectome Project, WU-Minn Consortium funded by the 16 NIH Institutes and Centers that support the NIH Blueprint for Neuroscience Research; and by the McDonnell Center for Systems

Neuroscience at Washington University. Support for analysis was also provided by the National Institute of Mental Health. Additional funding support was provided by the Ben B. and Iris M. Margolis Foundation.

CHAPTER 1

INTRODUCTION

Overview

Bioengineering is the application of engineering principles to biological or medical systems. Using a range of mathematical and analytical tools, bioengineers are represented in fields as diverse as materials science, drug development and delivery, artificial prosthetics, and medical imaging.

Medical imaging, specifically, gives us the opportunity to see inside the body and examine the structures and functions of myriad physiological systems noninvasively. The advent of magnetic resonance imaging (MRI) was a groundbreaking method of examining internal body structures, taking advantage of differences in magnetic susceptibility across different body tissues. The path toward development of MRI resulted in Nobel Prizes being awarded for advances in medicine and physiology. Most recently in 2003, Paul Lauterbur and Peter Mansfield were both awarded Nobel Prizes for their contributions to MRI development. Lauterbur received distinction for introducing gradients into the magnetic field that enabled visualization of two-dimensional structure. Mansfield was awarded the honor for demonstrating how signals from MR could be mathematically transformed into a coherent image, and for pioneering echo-

planar scanning in which rapid imaging occurs through rapid variations of gradients. Functional magnetic resonance imaging (fMRI) takes advantage of the differences between magnetic susceptibility in oxygenated versus deoxygenated blood, and allows us to track the progression of metabolic activity in the grey matter of the brain over time. This metabolic signal is known as the blood oxygen level-dependent signal, or BOLD signal.

The last two decades of functional MRI research has firmly rooted cognitive psychology in the biological systems of the human brain. Resting state functional connectivity (RSFC) in particular has paved the way for cognitively-driven research questions to become the subject of high-throughput biological methods. RSFC examines spontaneous fluctuations in brain activity, and determines the covariation of activity between regional pairs in the brain. Presently, RSFC studies represent a revolutionary phase for integrating behavioral data from research psychology with our rapidly increasing comprehension of dynamical systems in the human cortex. Empirical correlations between cortical physiology and human behavior will allow bottom-up assessment of the impact of neurobiology on behavior. This will have implications as diverse as philosophy of mind and translational medicine. This is also an important leverage point for correctly diagnosing, prescribing treatment, and monitoring a wide-range of clinical mental health and psychiatric disorders.

The fields of computer science and applied math have developed powerful solutions for large biological data made possible by the Human Genome Project and molecular assays such as genetic microarray technology. The current NIH

Human Connectome Project and the proliferation of large datasets for human functional connectivity in psychiatric typing and subtyping provide a parallel opportunity to integrate well-described engineering methods and to develop novel methods for formulating models of networks in functional neurobiology. To this end, I characterized components of human resting state functional connectivity patterns in large sample (n>1500) datasets, using cortical physiology captured through functional MRI time series data (BOLD signal).

A recurring strategy in my research is to explore principal components of RSFC by decomposing group-mean averages of RSFC, backproject vectorized principal components of RSFC onto anatomical space, and quantify dominant contributions to RSFC in a typically-developing population through network eigenvalues. Intuitively, we predicted at the outset that eigenvectors for RSFC matrices would correspond to primary cognitive functions such as primary sensory functions, internal attending, external attending, and language processing, with eigenvalues representing the proportion of cortical metabolism partitioned to each respective function. This prediction proved to be correct.

Complementary to functional architectural descriptions of whole brain activity, we set out to create a whole brain model of grey matter activity that could describe networks in the brain in terms of their transient stability. Because the brain is a dynamic organ, constantly adapting its flow of information and activity to accord with external sensory and cognitive demands, the goal was to approach the brain as a systems-based problem and characterize dynamic stability of transient intermediate states observed during normal brain function in

a typically-developing (TD) large sample population (n=500). We further compared intermediately stable configurations in functional patterns with established intrinsic connectivity networks in order to describe the functional connectivity of resting state neural activity in terms of fluctuating engagements between subdomains of canonical networks. We anticipated that resting state models of network dynamics would show group averages for large sample TD subjects that reflect intermediately stable states correspondent to hubs of established intrinsic connectivity networks, with overall convergence in resting state models to default mode network steady-state.

By quantifying neural dynamics, components, and stability of functional networks using high-throughput, large sample biological datasets integrating with information-rich behavioral assays for a large population (n=500), biomarkers in human cortical function may become the foundation of modeling human behavior and cognition in a way that corresponds to our current modeling of physical systems.

In a longitudinal interventional study, we explore the utility of RSFC for tracking neuroplastic modulation of long-term connections subsequent to behavioral training. In this specific paradigm, we used a speed reading behavioral training regimen. The principles of functional mapping and the demonstration of neuroplastic modulation in spontaneously occurring connectivity are a proof of concept, with the tools of analysis having potential application for tracking neuroplastic modulation of RSFC following any number of interventions, including tracking the effects of psychopharmaceuticals on whole brain function

(1). In the third study presented in this series, we demonstrate the ability of both traditional RSFC in addition to features from simulations of whole brain activity to mapping behavior and predicting cognitive and social characteristics of individual subject differences. This study in particular has the most exciting and direct potential application to translational clinical settings, as it presents novel methods for interpreting behavior mechanistically as behavior arises from supporting neurobiological functions. The goal beyond the methods put forward in the last study is to integrate behavioral predictions and brain network classification with diagnosis, prognosis, treatment planning, and therapeutic monitoring in medical clinical settings.

Background

Functional connectivity examines the architecture of physiological networks distributed across the grey matter (2-4). The roles of specific large-scale distributed networks have been robustly mapped for a wide range of experimental tasks, including facets of primary sensory perception, motor planning and execution, language processing, directed attention, and social reasoning. Functional connectivity MRI (fcMRI) originated with the discovery that metabolic synchrony between brain regions can be determined from blood oxygen level-dependent (BOLD) signal acquired over a series of successive time points (5). Resting state BOLD signal acquisition popularized the use of functional connectivity MRI to decipher distributed hubs of correlated metabolic activity when no outside task is imposed upon subjects. Largely, the

popularization of resting state fcMRI is due to the discovery of a major human neurophysiological network--the default mode network (DMN)—that was previously undescribed by other methods of physiological imaging (6). The identification of a previously unidentified network granted significant credibility to brain mapping as a tool for mechanically modelling the human brain and mind, given its ability to determine networks by biologically data-driven approaches, in contrast to reliance upon experimental task design to elicit a specific cognitive construct of interest.

To characterize the system of cortical networks that compose the human grey matter, independent component analysis (ICA) of BOLD signal fluctuations emerged as a leading methodological analytical tool (7-9). Spatially-independent sources of physiological signal as determined by ICA of BOLD time series sequences have been largely accepted as defining the core intrinsic connectivity architecture of large-scale spatially-distributed functional networks in the human brain recorded across the whole brain are reasoned to represent fundamental distributed networks. Intrinsic connectivity between spatial regions of the brain was observed to be highly consistent, and resulted in the conclusion of a network architecture highly reproduced across healthy control subjects (4, 10). It logically became a focal point of investigation to determine whether variations in the brain's independent components are descriptive of mental health and psychiatric state.

There is converging evidence that functional connectivity MRI faithfully reflects underlying neurobiological substrates. Honey et al. demonstrated that

functional connectivity MRI is aligned with information from structural connectivity such as diffusion tensor imaging (11). In a study comparing functional connectivity to patterns of activation seen across thousands of reported brain imaging studies, it was noted that functional network boundaries identified by functional connectivity closely matched those obtained from a meta-analysis of published coordinates from the Brainmap database (12). Such observations have led to the conclusion that functional connectivity is sufficiently constrained by structural connectomics in the brain as to be a reliable metric of functional brain organization (13).

Principal components analysis (PCA) of functional grey matter correlations have been analyzed with some success to characterize the functional partnering of nodes across intrinsic networks, while additionally providing a promising series of additional biomarkers for neurophysiological disease (14). PCA differs from ICA in RSFC in that more spatially distributed information is obtained as opposed to the localized brain networks obtained from independent component analysis. While ICA is effective at obtaining parcellations of the brain (15), it may be less sensitive to brain components that integrate or contrast information from different brain networks that are important for both normal brain function and pathophysiology in disease.

With the aggregation of pattern recognition methods becoming commonplace in brain mapping data, the current need is to assemble biologically-based classification systems whose usefulness could make the translational step into clinical application, most probably by means of diagnostic

screening, prognosis, and guidance of treatment for neuropsychiatric illness. Initial studies at classifying disease states have moved beyond early efforts at distinguishing group means (16, 17) to more sophisticated classification algorithms using whole brain connectivity patterns and multisite datasets (18, 19). Nevertheless, previous literature does not support a robust clinical use of clinical diagnostic biomarkers that have been proposed to date, and this is an area of active research and pressing clinical need. In fact, the NIMH included in its new strategic plan to “Develop, for research purposes, new ways of classifying mental disorders based on dimensions of observable behavior and neurobiological measures” (20).

The complexity of nonlinear dynamics to describe neurophysiological relationships has inhibited its development in biomarker development. Nonetheless, the dynamic stability of functional networks have been demonstrated through biologically-based simulations to have potential as functional biomarkers (21). Increased understanding of the behaviors of transiently stable functional states in the brain will allow us to examine variations in neurobiology from a different angle and establish quantitative metrics for the behavior of transient stability in functional connectivity.

Current work in the field is exploring sliding temporal windows to BOLD time series data to quantify the variation of functional correlations themselves over time (22, 23) and using temporal mixing functions (24). Although provocative, these approaches are plagued by signal processing challenges of obtaining satisfactory signal from noise separation owing to the reduced number

of time points considered in current sliding temporal window methods. Intuitively, one would expect the brain's functional correlations would be described better as a nonlinear system with fluctuating correlations between regions based on specific environmental and task demands. And indeed, a growing body of studies confirm that functional correlations observed as averaged values across long time series are not correspondent with moment-to-moment strengths in coordination between regions of the brain (25).

MR signal filtering remains an ongoing methodological evolution in brain mapping, advancing the field in this direction via superior acquisition sequences, forays into higher-power scanner magnets (7 T and above), and optimized filtering remain priorities (23, 26). As previously mentioned, rich temporal fluctuations of nonlinear interactions describe low-frequency functional connectivity in the human brain. The scientific questions alone regarding the functions of these complex signals are titillating. Added to the translational impact in understanding and treating disease, it becomes important to develop suitable techniques for maximally precise single-subject brain analysis. Functional connectivity adjacency matrices have demonstrated longitudinal reproducibility in single-subject trials (27-29). This gives confirming evidence to the likelihood that even static averages of functional connectivity in single-subject acquisitions show potential for clinical used in personalized neurological and psychiatric medicine in the domains of diagnosis, prognosis, and guidance of treatment.

A landmark study using resting state fMR images from 1,000 subjects demonstrated clusters of functionally-related, spatially-distributed network hubs,

with optimized parcellations at 7-network divisions and 17-network divisions (4). This invokes tautological questions about defining a “network.” Competing experimental analyses for network divisions explicitly caution against premature conclusiveness of intrinsic connectivity findings owing to ongoing refinement of methods for data filtering and BOLD signal processing (30). Unsettled controversy notwithstanding, significant findings from interspecies comparisons of functional architecture in cortex of humans versus monkeys shows immense expansion of association cortices in humans over other primates (4). This gives provocative insight to the emergence of cognitive capacities unique to Homo sapiens amongst the primate family, particularly as networks involving association cortical regions do not demonstrate perceptible hierarchical organization.

The current proliferation of high throughput biological data has been likened optimistically to the scientific moment in astronomy when the telescope was adopted as a standard research tool (31). By collecting high throughput biological data and monitoring physiological functions across time, we gain the ability to describe biological systems with precision approaching physical mechanical systems modeling. The NIH Human Connectome Project fills an important gap in currently available research data capable of building these models to incorporate the three domains of physiology, behavior, and genetics. (32, 33, 34, 35).

Impact of Current Research

My research is innovative in several ways. First, characterization of the principal components of functional network connectivity in humans has not been completed in a large dataset akin to the HCP500 project, nor has rearrangement of principal components from task-driven effects been characterized. While there have been prior reports evaluating relationships between functional connectivity and behavioral metrics (32, 33), prior reports have used limited datasets with small sample sizes and low temporal resolution that limit ability to discriminate individual phenotypes. The Human Connectome Project dataset provides the first opportunity for large-sample, high-quality functional connectivity evaluation of personality and other behavioral metrics in a typically developing cohort. Second, this project moves the field of functional connectivity research toward deriving biological markers for canonical neuropsychological and psychiatric diseases. Defining biomarkers in a typically developing population allows determination of canonical variants of human behavior that can be applicable to any disease population for which there is an adequate sample size to examine. Third, the early development of biologically-based neural markers for behavior and neuropsychiatry creates a new way for integrating imaging genetics with neurological and psychological assessment.

Fourth, these projects extend a method for dynamical evaluation of brain network stability. Presently, dynamical evaluation of brain networks has been approached from static concatenation of brain microstates or temporal independent component analysis (22, 24). A true dynamical stability assessment

of attractor kinetics of brain networks (21) has not been applied to modern functional connectivity data with extended imaging time per subject and allows the opportunity for characterization of brain network stability and metastability.

Approach to Functional Connectivity

For simplicity, resting state functional connectivity is often modeled as a static set fixed parameters describing the strength of pairwise correlations throughout the brain. The true behavior of the physiological system is more complex, and involves fluctuating combinations of pairwise correlation strengths influenced by internal and external demands. To understand the effects of task-driven demands on network physiology, we explored group-level changes in functional architecture of the brain in response to tasks performed by participants while being scanned, including gambling, cognitive, emotional, and social-based tasks. We demonstrate that principal components of the functional connectome change in association with external task demands, reflecting preferential recruitment of physiological networks supporting cognitive processes demanding by respective task states.

Typically, functional connectivity has been measured by calculating the correlation coefficient between BOLD time series in different brain regions or networks (5, 3). Alternately, approaches in the frequency domain have used coherence to similarly identify a relationship between the two time series (62). Nonlinear metrics of synchrony between the time series, such as mutual information, have also been described (63). Yet while these approaches can

establish a relationship between two regions that presumably incorporates information about underlying structural connectivity between the regions, it also may include information about shared connections with a third region. For our purposes, we would like to improve the quantitative relationships of connectivity between brain regions by attempting to account for such indirect connections. One method that has been used for approximating direct connections only is to regress out the effects of all other brain regions using partial correlation (64).

Limitations and Future Research Opportunities

Because all participants are recruited from the United States, there may be limitations in generalizing conclusions of preferred network architecture, recruitment, and behavioral prediction across cultural variables. This is significant since higher cognitive functions (most obviously language) are largely reliant on socialization factors for their full expression. Across disease states, as well, it is possible that brain networks and neurophysiological recruitment may be altered enough to prevent the direct comparisons against healthy control characterization that we currently anticipate. To the contrary, modulations in functional architecture affiliated with disease states might be subtle enough in the spatial redistribution that current acquisition and analytic methods may need to be further refined to compensate for challenges in spatial resolution of data. Conclusions for behavioral and physiological integration also need to be recognized as possibly lacking enough density and precision in subcortical mapping to truly account for contributions of subcortical architecture and variation

to healthy network function and the role of subcortical regions in supporting behavior. The limitation is compounded by the difficulty of computational tractability for dense matrix calculations in second-order connectivity analyses, since the size of computational data expands geometrically between first- and second-order approaches.

An immediate follow up investigation to this project will examine the application of dynamic mapping and brain-behavioral modeling to clinical categories, including autism, ADHD, Down Syndrome, and bipolar disorder with the aim to develop clinical diagnostic biomarkers for these conditions. Upon completion of in silico brain models for resting state healthy control subjects, we will begin to look at intentional perturbations in the physiological system and move toward comparisons between simulated responses from healthy control models versus responses of disease-related parameters of whole brain physiology, motivated by both basic science understanding of disease in addition to continued establishment of reliable biomarkers for healthy and pathological variations of functional architecture. Additionally, future work involves triangulating genetic data with behavioral and physiological information from HCP participants in order to integrate imaging genetics into the brain-behavioral correlative analyses.

Elucidating the dynamic relationships between genetics, cortical function, and behavior promises to reveal new fundamental understanding about what makes us uniquely human and what makes each person different from others (34).

CHAPTER 2

DYNAMICAL STABILITY OF INTRINSIC CONNECTIVITY NETWORKS[1]

Abstract

Functional connectivity MRI (fcMRI) has become a widely used technique in recent years for measuring the static correlation of activity between cortical regions. Using a publicly available resting state dataset (n=961 subjects), we obtained high spatial-resolution maps of functional connectivity between a lattice of 7266 regions covering the gray matter. Average whole brain functional correlations were calculated, with high reproducibility within the dataset and across sites. Since correlation measures not only represent pairwise connectivity information, but also shared inputs from other brain regions, we approximate pairwise connection strength by representing each region as a linear combination of the others by performing a Cholesky decomposition of the pairwise correlation matrix. We then used this weighted connection strength between regions to iterate relative brain activity in discrete temporal steps, beginning both with

[1] Reprinted from NeuroImage, Vol 59/4, Michael A. Ferguson, Jeffrey S. Anderson, Dynamical Stability of Intrinsic Connectivity Networks, 4022-4031, Copyright (2012), with permission from Elsevier.

random initial conditions, and with initial conditions reflecting intrinsic connectivity networks using each region as a seed. In whole brain simulations based on weighted connectivity from healthy adult subjects (mean age 27.3), there was consistent convergence to one of two inverted states, one representing high activity in the default mode network, the other representing low relative activity in the default mode network. Metastable intermediate states in our simulation corresponded to combinations of characterized functional networks. Convergence to a final state was slowest for initial conditions on the borders of the default mode network.

Introduction

Functional connectivity MRI (fcMRI) examines the synchrony of slow-wave fluctuations in BOLD signal (<0.08 Hz) between geographical regions in the brain, and infers common functional relationships when correlated BOLD time series exist between regions of interest (ROIs) (2, 3, 5, 35). Similarly, antagonistic relationships between regions are inferred from anticorrelations in their respective BOLD signal fluctuations over time (36, 37), when not induced by postprocessing strategies (38-40).

fcMRI methods were first used to map the sensorimotor cortex of the resting human brain (5), with subsequent investigations demonstrating consistent intrinsic connectivity networks detectable by fcMRI during wakeful rest (7, 41-46). Recent anatomical work within resting state functional connectivity analysis has benefitted from large datasets from multiple centers. In conjunction with the

Neuroimaging Informatics Tools and Resources Clearinghouse (NITRC) and the International Neuroimaging Data-sharing Initiative (INDI), a large scale resting state fMRI dataset has already been made openly accessible through the 1000 Functional Connectomes Project (2) containing resting state fMRI data obtained from over 1400 subjects by 28 international laboratories.

Among the most robust distributed connectivity networks is the default mode network (6, 47), comprised from brain regions that are consistently more active during wakeful rest than during numerous cognitive tasks (48). These observations led to the hypothesis that this network of regions might be supporting default activity of the human brain (6, 45, 49), such as attending to internal stimuli, self-reflection, or internal narrative (49-51).

Despite such extensive work on clarifying the functional network anatomy of the brain, there are yet relatively few reports attempting to extend static connectivity measurements to whole brain dynamical models (52). One approach used known structural relationships in the macaque brain from anatomical tracing studies to simulate interactions of neural oscillators in each region using weak coupling coefficients (53). Another approach using macaque connectivity demonstrated ultraslow coherent network fluctuations in a model using anatomic connectivity, time delays, and noise (54). The relationship of anatomic topology, coupling strength, time delay between regions, and noise to temporal dynamics was further explored in a report using a network of Wilson-Cowan modulators to simulate slow coherent fluctuations (55).

One limitation of such approaches to network modeling is that precise information from anatomical tracer studies is not available for the more complex human brain, and precise path lengths and anatomic topology are difficult to measure. Also, the complexity of connectivity between regions becomes computationally intractable with the number of nodes studied in a dynamical network. As an alternate approach, we investigate a dynamical model that treats as computational units regions of gray matter on the scale of several millimeters. Rather than build neural networks from high temporal-resolution oscillations, we use an iterative approach at discrete time points to evaluate dynamical relationships between large-scale distributed networks. We report that using only functional connectivity measurements between a lattice of brain regions covering the gray matter, the brain's default mode network emerges in such simulations as a dynamically stable state, with other described intrinsic connectivity networks demonstrating reproducible metastability across a wide range of initial conditions.

Materials and Methods

fMRI Data Sources

fMRI data was extracted from the open-access '1000 Functional Connectomes Project' (http://fcon_1000.projects.nitrc.org/) in which resting-state fMRI scans have been aggregated from 28 sites. (2) For inclusion we required whole-brain coverage from MNI coordinates z=-35 to z=70. Any subject for whom postprocessed data did not cover all 7266 ROIs was discarded prior to analysis. Although postprocessing steps were performed using an automated batch, the

results of normalization, segmentation, and realignment steps were manually inspected for all subjects, and any subject for whom the normalized and segmented images were not in close alignment with the MNI template on visual inspection were discarded. The Dallas sample was not included because of ambiguity about left/right orientation at the time of analysis. From 1051 subjects for whom batch postprocessing was initiated, 961 subjects from 23 sites were included in the analysis sample. The datasets from which these subjects were obtained are listed in Table 1. Mean age of the subjects was 27.3 +/- 11.7 s.d. years (range 13-79). 525 subjects were male, 394 female, and gender of 42 subjects was unknown.

Additional data from a single subject was also analyzed. Data from this subject have been previously published (56), although analyses presented herein are unique to this report. For this subject, (male, 39 years old), eleven scan sessions were obtained. In six of the sessions, the subject was watching cartoons (Looney Tunes Golden Collection, Volume 1, Warner Brothers) for ten 5-minute BOLD scans per session (50 minutes BOLD data per session). In the other 5 sessions, 50 minutes of resting BOLD data was obtained (10 5-minute scans, eyes open).

fMRI Post-Processing

The following sequence was used for image post-processing of all BOLD image datasets. Using SPM8 toolbox (Wellcome Trust, London), BOLD images were realigned (realign, estimate and write), coregistered to MPRAGE image

Table 1: Reading Comprehension

	Mean	*Standard deviation*
Age (n=9)	*18*	*2.3*
GORT-4 comprehension	*10.6 (63 percentile)*	*1.7*
GORT-4 fluency	*13.2 (84 percentile)*	*3.0*
Scan interval	*6 mo.*	*2 mo.*

(coregister, estimate and write), and normalized to MNI template (normalize, estimate and write, T1.nii template). Gray matter, white matter and CSF were segmented from MPRAGE image using SPM8 segment function (modulated, normalized, thorough clean). Images were bandpass filtered between 0.001 and 0.1 Hz and a linear detrend was performed at each voxel in the brain. Because each site used slightly different TR, we note that this detrend step may introduce some heterogeneity of filtering between sites associated with the detrend operation. Time series were averaged from 2 ROIs in the white matter (bilateral centrum semiovale, CSF (lateral ventricles), soft tissues of the head and face, and 6 rigid motion correction parameters from realignment step as previously described (40, 57) and for each voxel, a general linear model was used to find a best fit for white matter, CSF, soft tissues, and motion parameter time series,

which were subtracted from the voxel's time series. No regression was performed of the global signal or gray matter.

Methods for Calculating Connectivity

Typically, functional connectivity has been measured by calculating the correlation coefficient between BOLD time series in different brain regions or networks (3, 5). Alternately, approaches in the frequency domain have used coherence to similarly identify a relationship between the two time series (58). Nonlinear metrics of synchrony between the time series, such as mutual information, have also been described (59). Yet while these approaches can establish a relationship between two regions that presumably incorporates information about underlying structural connectivity between the regions, it also may include information about shared connections with a third region. For our purposes, we would like to improve the quantitative relationships of connectivity between brain regions by attempting to account for such indirect connections. One method that has been used for approximating direct connections only is to regress out the effects of all other brain regions using partial correlation (15, 60). We used both full correlation, partial correlation, and a novel method using the Cholesky decomposition of the correlation matrix between brain regions to estimate direct connections between brain regions. Details for these methods are given below.

Calculation of Full and Partial Correlation Matrices

An MNI template for gray matter (SPM8, grey.nii, intensity >0.5) was parcellated into 7,266 regions of interest (ROIs) by removing voxels from the image that were less than 5 mm from other retained voxels. Then all gray matter voxels were assigned to the closest remaining voxel's ROI. The ROIs ranged from 2 to 12 voxels in extent (mean 4.9 +/- 1.3 voxels at isotropic 3 mm resolution). Time series data for each ROI were generated from the averaged time series of all voxels pertaining to the respective ROI. Postprocessed time series data from every ROI were compared to the time series from all other ROIs using Pearson correlation coefficients. The resultant 7,266 by 7,266 matrix of correlation coefficients constituted a whole-brain functional correlation matrix for an individual subject. The whole-brain correlation matrices for each subject were Fisher transformed by evaluating hyperbolic arctangent to improve normality (36) and averaged across all subjects to produce a mean full correlation matrix.

The mean full correlation matrix was converted to correlation values by reverse Fisher transformation, and partial correlation values were obtained using method of Marralec et al. (15, 60). We inverted the full correlation matrix C_{ij} to obtain $Y_{ij} = C^{-1}$. Partial correlation coefficients P_{ij} were obtained by the relationship:

$$P_{ij} = - Y_{ij} / \text{sqrt}(Y_{ii} Y_{jj}) \quad [1]$$

Decomposition of Functional Correlation Matrix

Correlation coefficients can measure synchrony between two time series, but are only an indirect estimate of anatomic connectivity (11). One reason for differences is that shared inputs to two regions contribute to correlation values. For example, if two regions x and y had no direct relationship, but both exhibited positive correlation with a third region z, it would be expected that x and y would nevertheless show significant positive correlation.

We approached this problem by considering a linear model in which we start with an intrinsic noise time series $A_{it} = [a_i(t)]$ for region i and time point t and a transition matrix $T=[t_{ij}]$ of coefficients representing connectivity between region i and region j. A is constructed to have mean 0 and standard deviation 1 for each row by subtracting the mean and dividing by the standard deviation. For m regions and n time points, A will represent an $m \times n$ matrix, and T will represent an $m \times m$ matrix such that:

$$TA = B \quad [2]$$

where B will be an $m \times n$ matrix where row i represents a time series for region i, simulating a BOLD time series. The correlation between rows b_i and b_j should approximate c_{ij}, the measured correlation value from actual BOLD time series between region i and region j. Then we assign matrix $C = [c_{ij}]$ as the dot product of the rows of B:

$$T A A' T' = n C \quad [3]$$

But A represents an intrinsic noise signal for each node which should be independent for each row. For sufficiently long time series *A* of length *n*, since the rows $a_i(t)$ are independent with uniform standard deviation, then $A\,A'$ will approximate the identity matrix times the length of the time series n and we must find a matrix *T* such that

$$T\,T' = C \quad [4]$$

But this equation is known to have a unique solution *T* that is upper triangular if and only if *C* is positive definite (61), and this solution can be obtained from the Cholesky decomposition of *C*. We designate t_{ij} for $i>j$ as the approximated connectivity between region *i* and region *j*, and constructed the weighted connectivity matrix used in the analysis by setting $t_{ji} = t_{ij}$ for $i>j$ and normalizing each row of the matrix by subtracting the mean and dividing by the standard deviation. Cholesky decompositions were performed using the standard Matlab function chol.m.

To show with simulated data how the Cholesky decomposition may be related to individual time courses from brain regions, we generated 7266 intrinsic noise time series of length 1000 time points (matrix *A*, 7266 x 1000). To better simulate BOLD data (62, 63), these noise time series were generated with each row having mean 0 and standard deviation 1, with 1/f frequency distribution (pink noise) using the method of Little et al. (64). The 7266 x 7266 correlation matrix was averaged across all 961 subjects after Fisher transformation, and the mean was converted back to correlation values by evaluating the hyperbolic tangent. Cholesky decomposition matrix T was obtained and simulated BOLD time series

(matrix *B*) was generated from the matrix product in [2]. Pearson correlation coefficients were obtained between each pair of rows in *B* and a 7266 x 7266 matrix of correlation values was obtained. This process was repeated 1000 times, with the resulting correlation matrix averaged across trials after Fisher transformation with results shown in Figure 1.

Compared to the actual measured BOLD correlation values, there is close agreement to the time series *B*, representing a linear combination of independent noise vectors as specified by the transformation matrix T generated by the Cholesky decomposition. Thus, a biophysical model in which one considers each brain region to have intrinsic fluctuations (noise) that combine with the intrinsic activity of other brain regions according to a weighted connectivity matrix T will generate time series with correlation matrix C satisfying Equation 4.

Whole Brain Functional Simulations

To model brain activity over time, each of the 7,266 ROIs was assigned a pseudorandom value from a normal distribution with mean 0 and standard deviation 1. These starting conditions were considered ‘step 0’ of the simulation. For step 1 of the simulation, the intensity values at every ROI of the brain were assigned by considering every other ROI’s intensity value from the previous step, multiplying that intensity value by its respective weighted connectivity coefficient, then summing the products of intensity and connectivity values in order to determine the new intensity value at each ROI. The simulation was repeated for 5,000 sets of randomized initial conditions, with 40 steps in each simulation.

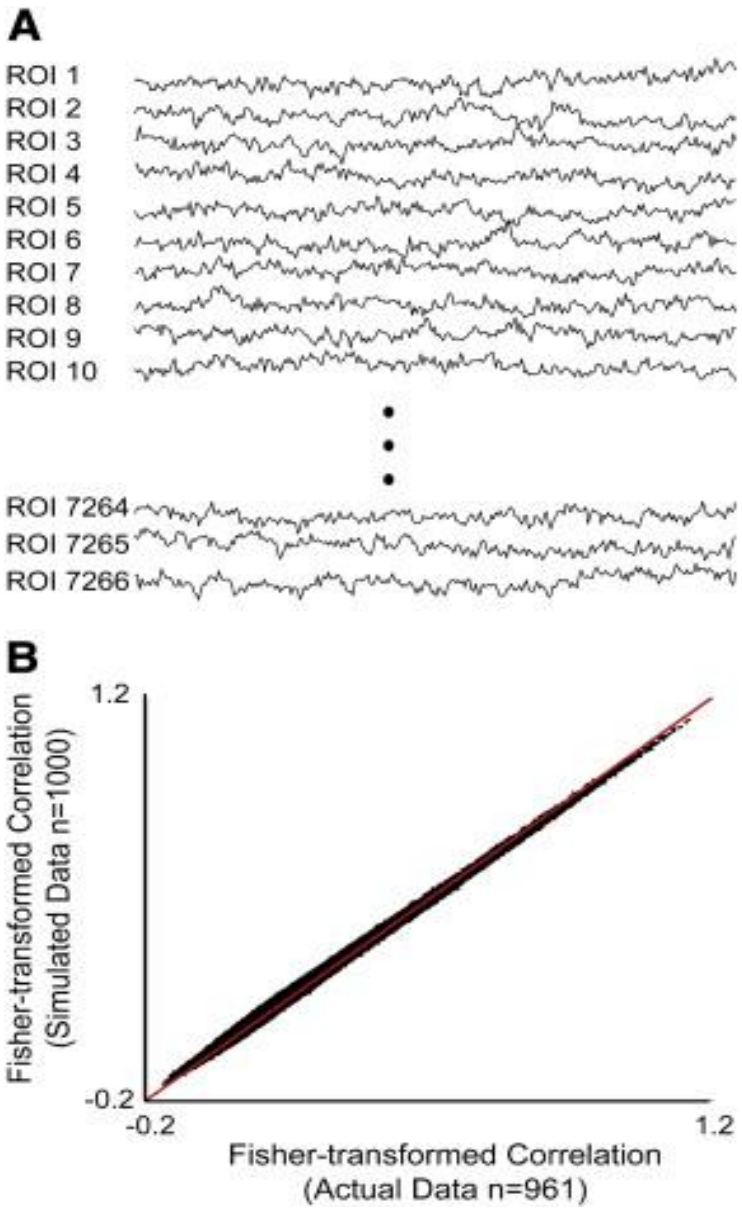

Figure 1: Simulating correlated BOLD data using Cholesky decomposition. **A)** Intrinsic noise time series were independently generated for 7266 ROIs (1000 time points per ROI), such that each time series showed a 1/f distribution, with 0 mean and 1 standard deviation (matrix A from [1]). **B)** Comparison of Fisher-transformed correlation for each connection from actual measured data with simulated correlation. Simulated correlation was obtained by the Pearson correlation coefficient between each row of TA, where T is the matrix obtained from the Cholesky decomposition. Y-axis shows the mean correlation values of 1000 trials, averaged after Fisher transformation. Red line shows y=x.

Identifying and Categorizing Metastable States

The rate of change in neural activity between steps in the whole brain simulation was determined by finding the sum of the absolute values of intensity differences between corresponding ROIs for successive steps. Metastable patterns of neural activity were identified by local minima in the rate of change. Each of the metastable states across all 5,000 iterations were clustered using the dendrogram.m function with city block p-distribution and average linkage using the MatLab statistical toolbox (R2010b). The characteristic networks for each cluster was determined by calculating the mean for all metastable states within the same dendrogram cluster.

Determining Convergence

In addition to the 5,000 whole brain simulations in which randomized starting conditions were assigned to each of the 7,266 ROIs, we performed an additional 7,266 simulations using parameters obtained from resting state functional correlation measurements as the starting conditions. In this paradigm, the whole brain initial conditions for each iteration were set to the correlation values corresponding to the seed from one of the respective 7,266 ROIs. For each set of 7,266 initial conditions corresponding to a different ROI seed, we measured the number of steps in the simulation required for the system to converge to within a tolerance of less than 0.05% change in the mean absolute value of the intensity across the ROIs. The scalar corresponding to the number of

steps for convergence for each seed ROI was then assigned to the respective ROI, and mapped onto a gray matter whole brain image.

Results

To determine a standard map of functional correlation, we averaged pairwise functional correlation measurements between 7266 brain regions of interest (ROI) covering the gray matter for 961 healthy adult control subjects available through the open access 1000 Functional Connectome Project resting state database. Regions were selected by parcellating an image of brain gray matter (SPM8 toolbox, Wellcome Trust, London, grey.nii) into regions such that each region's center was at least 5 mm distant from every other region, effectively yielding ROIs of 5 mm diameter (65, 66). Pairwise correlation measurements between these regions comprised 26.3 million connections for each subject.

Reproducibility of Functional Correlation Measurements

Before attempting dynamical modeling, we characterized the reproducibility of the functional correlation measurements by comparing mean correlation values for a randomly selected subsample of the total control population (Figure 2A) compared to a different unique subsample of the same size. Subject subsamples of all sizes showed a normal distribution of connectivity differences between groups, with standard deviation of the error inversely proportional to the square root of the number of subjects averaged (Figure 2B).

When we divided the sample into 2 groups of 480 and 481 subjects, we observed close agreement of correlation values for all 26.3 million connections (Figure 2C), indicating consistent reproducibility of functional correlation outcomes for large population samples from the 1000 Functional Connectomes database. The mean pairwise functional correlation matrix is shown in Figure 2D. By extending the relationship seen in Figure 2B, we estimated that each individual measurement between 2 ROIs had an accuracy of less than 0.01 units of Fisher-transformed correlation compared to what would be expected for a similarly constructed population of 961 subjects.

Weighted Connectivity Calculations

Correlation measurements, however, are only an approximation of the expected connectivity strength between two regions, and may be systematically misleading by incorporating shared input from other regions in a pairwise correlation measurement. We attempted to adjust for this relationship by approximating relationships between regions using a Cholesky decomposition of the pairwise correlation matrix as described in the Methods section, wherein weighted connectivity between regions more closely approximates what would be expected if each region were expressed as a linear combination of the other brain regions. We subsequently refer to this pairwise association matrix after Cholesky decomposition as the weighted connectivity matrix between regions.

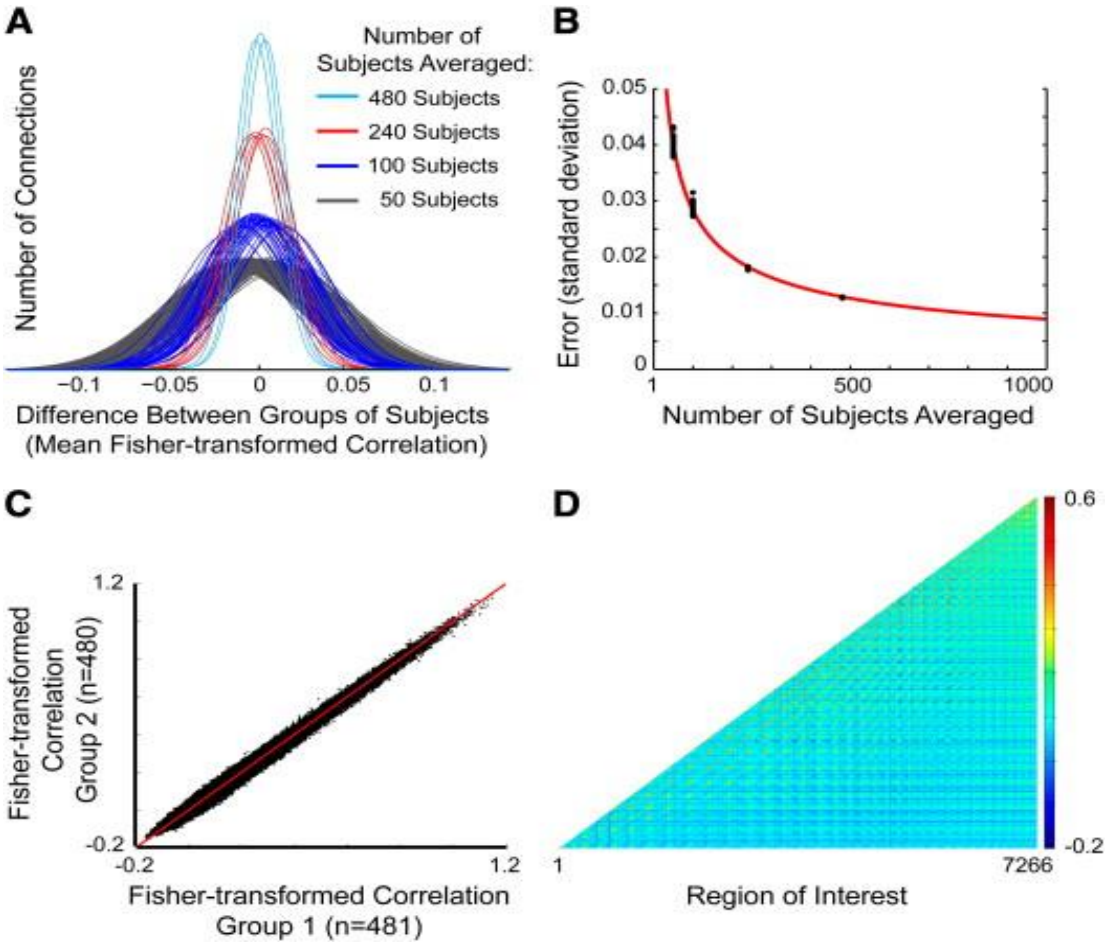

Figure 2: Reproducibility of functional correlation measurements. **A)** Distributions of the difference in correlation between randomly selected subsamples of subjects across all 26.3 million connections. Subsets of 50, 100, 240, or 480 subjects were compared. Each histogram shows for two unique subsamples of the population the distribution of difference in mean correlation across all connections between the two groups. **B)** Standard deviation of difference in correlation across all connections as a function of the number of subjects averaged. The y-axis represents the standard deviation of difference in mean correlation across connections for two subsamples of the population. The standard deviation for each connection across all subjects was averaged across connections and was 0.2828. The red fitted curve is 0.2828/sqrt (number of subjects). **C)** Comparison of mean Fisher transformed correlation values from 2 unique subsamples of 480 and 481 subjects. Red line shows y=x. **D)** Pseudocolor plot showing mean Fisher transformed correlation values for connections between each ROI. Color range was limited to -0.2 to 0.6 to optimize image contrast.

To compare the results of the Cholesky decomposition solution with the original measured functional correlation data as well as with partial correlation analysis, we used seed voxels from three major networks of interest (default mode, attention control, and primary auditory networks) to illustrate the effect of the method on known intrinsic connectivity networks. For each of the seed voxels, the weighted connectivity measurements from the Cholesky decomposition demonstrated higher specificity of interregional relationships than was shown by full correlation of time series data shown in Figure 3.

When compared to partial correlation measurements, the Cholesky decomposition results show greater similarity to partial correlation than to full correlation seen in Figure 4, with many values close to zero in both partial correlation that had larger positive or negative values in full correlation analysis. This presumably reflects connections that have shared correlation with other brain regions but weak or absent direct connection. Cholesky decomposition differs from partial correlation in our data in that partial correlation shows near complete absence of long-distance connections, while such long-distance connections are largely preserved in the Cholesky method.

Whole Brain Simulation and DMN Convergence

We then used the weighted connectivity matrix derived from Cholesky decomposition to create a simulation of the brain using a two-step iterative

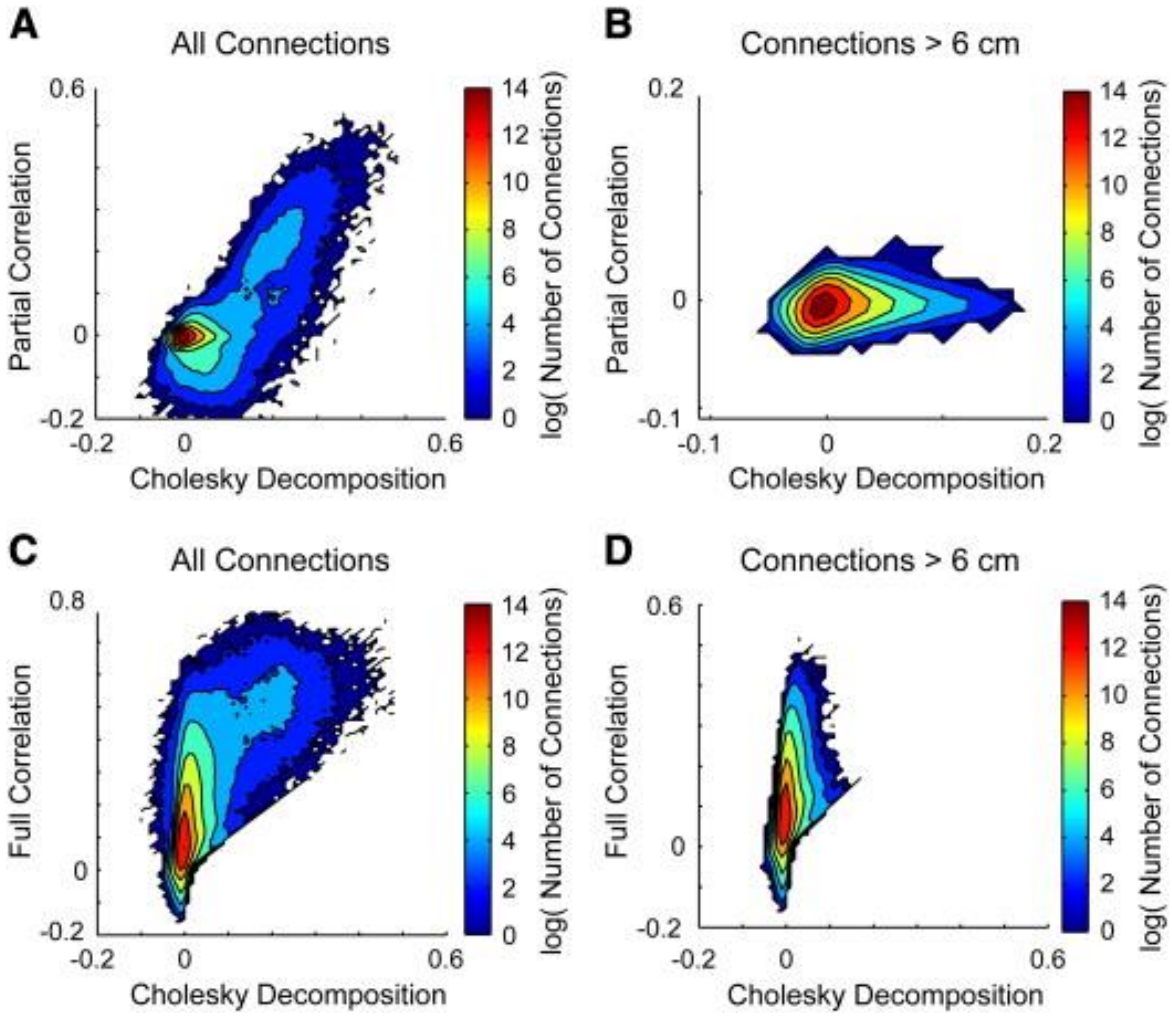

Figure 3: Effect of Cholesky decomposition on intrinsic connectivity networks. To the left are shown Fisher-transformed full correlation values of each ROI to 3 seed ROIs in the posterior cingulate, left intraparietal sulcus, and left primary auditory cortex. Corresponding values of the weighted connectivity matrix (Cholesky decomposition) are shown in the center column for the same seeds. Partial correlation values are shown in the right column for the same seeds. Images were normalized by subtracting the mean and dividing by the standard deviation across ROIs, with color showing standard deviations across ROIs for better comparison of image contrast in the three techniques.

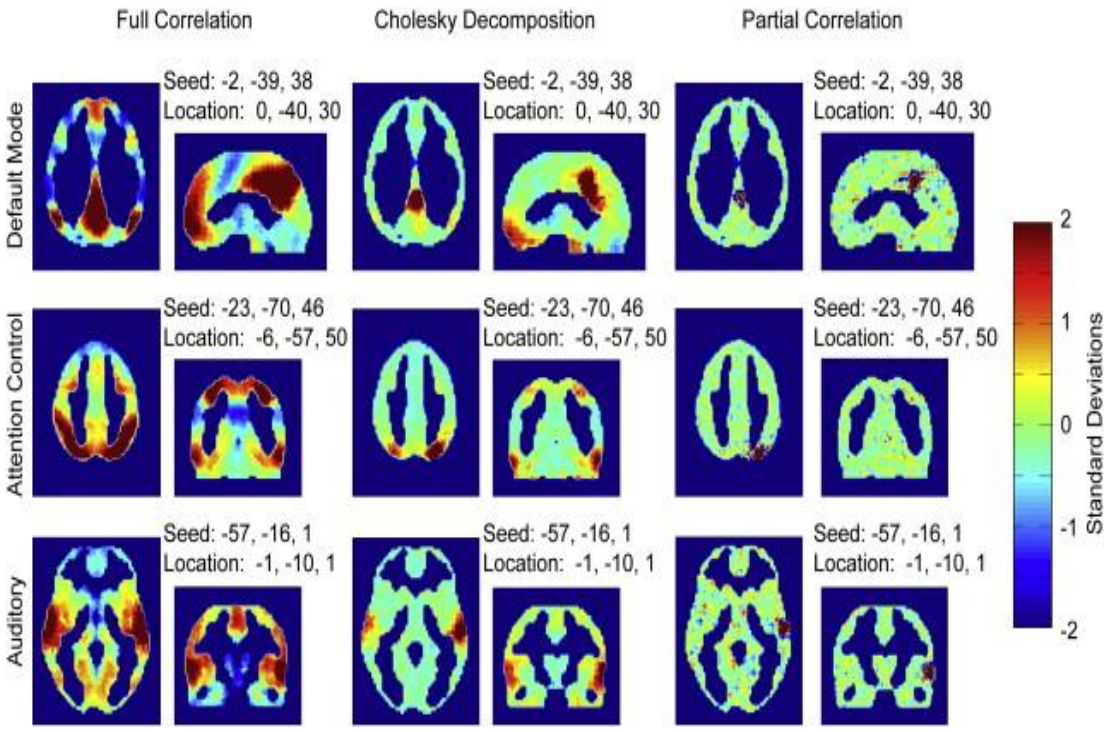

Figure 4: Density maps comparing distribution of full correlation, Cholesky decomposition, and partial correlation techniques. **A)** Distribution of Cholesky decomposition vs. partial correlation. Color scale shows filled contour plots of the logarithm of the number of connections in each bin. Bin size was 0.01 in each axis. **B)** Density of Cholesky decomposition vs. partial correlation showing only connections between ROIs greater than 6 cm apart in Euclidean distance. **C)** As above, comparing Cholesky decomposition with full correlation. **D)** Cholesky decomposition vs. full correlation for connections between ROIs greater than 6 cm apart.

process. First, the “activity” of an ROI at any step in the simulation is the weighted sum of the activity values of all other ROIs from the previous step multiplied by their weighted connectivity coefficient with the ROI. Second, the resulting values were normalized across the brain by subtracting the mean activity across all brain regions and dividing by the standard deviation of activity across brain regions. The normalization step prevents any one brain region from achieving unrealistically high or low activity. The simulation models what might be expected where brain activity in one step is determined by *relative* brain activity in the previous step in addition to the information in the weighted connectivity matrix. We repeated the simulation using 5000 randomized initial conditions in which initial brain activity was selected from a normal probability density function with mean 0 and standard deviation of 1. Each of the 5000 iterations showed stable convergence by 40 steps in the simulation (Figure 5A & 5B) with robust convergence to the default mode network in 4955 of the simulations (Figure 5C).

Forty-five of the 5000 simulations converged to a different stable state characterized by high activity in the visual network consisting of the occipital lobe and posterior medial parietal lobe. The simulations that converged to the default mode network were distributed roughly equally between states where the default mode regions converged to positive activity and states where the default mode regions converged to negative activity, since a simulation converging to negative activity is identical to a simulation converging to positive activity with the sign of

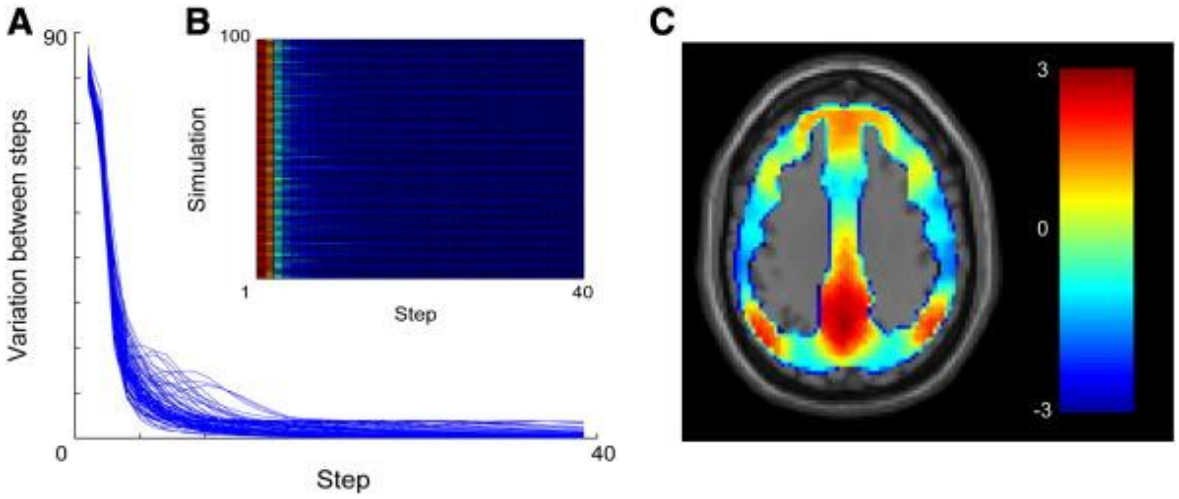

Figure 5: Convergence to the default mode network. **A)** Difference between steps for each of 100 simulations from random initial conditions, measured as the sum of absolute value of differences between normalized intensity values at each ROI between the two steps. Only a subset of the simulations is shown to better allow visualization of traces. **B)** Pseudocolor plot showing difference between steps for the same 100 simulations. **C)** Final convergence state for one of the simulations. Colors represent normalized activity across ROIs. All of the final convergence states from these simulations were qualitatively identical or an additive inverse of the image shown (negative values where positive values are shown) although in a minority of simulations (<1%) the final convergence state was instead the visual network.

all initial conditions inverted. The convergence to the default mode network during weighted connectivity-based simulations was robust across resting state data subsets from acquisition sites, and not a unique characteristic of the whole set average. The weighted connectivity matrices specific to the two largest data subsets (Beijing n=188, Cambridge n=194) both demonstrated robust convergence to the default mode network during whole brain simulations based on their respective weighted connectivity matrices with only slight differences in final convergence state.

Single-Subject Reproducibility, and Task-Specific Influence on Whole Brain Simulations

In order to assess the scalability of weighted connectivity-based whole brain simulations to the single-subject level, we acquired resting state data from a healthy control subject for five, one-hour blocks. The BOLD time series from each of the five, one-hour blocks was processed as previously described in order to create weighted connectivity matrices for each of the five, one-hour resting state acquisitions. The convergences to steady-state brain activity demonstrate robust, reproducible default mode network configurations for each of the five, one-hour datasets on the same subject shown in Figure 6B. Further, when the same subject was instructed to watch cartoons for six additional, one-hour periods, the steady-state convergence patterns from each of the weighted

Figure 6 Convergence states for a single subject. **A)** Each row represents the final convergence state from data obtained from 50 minutes of BOLD imaging while the subject was watching cartoons during an independent imaging session. (Figure 6 Continued) **B)** Each row represents final convergence state from data obtained from 50 minutes of BOLD imaging in a resting state, eyes open. **C)** For each 50-minute session, the final convergence state was measured as a vector of activity across 7266 ROIs. The plot shows correlation coefficients between the activity vector for each pair of sessions. Pairs of unique sessions were more similar for when subjects were watching cartoons in both sessions ($r = 0.71$) or resting in both sessions ($r = 0.68$), than when one session was watching cartoons and the other was in the resting state ($r= 0.43$). A two-tailed t-test comparing correlation coefficients for different tasks vs the same task was significant at $p = 1.9 e -17$).

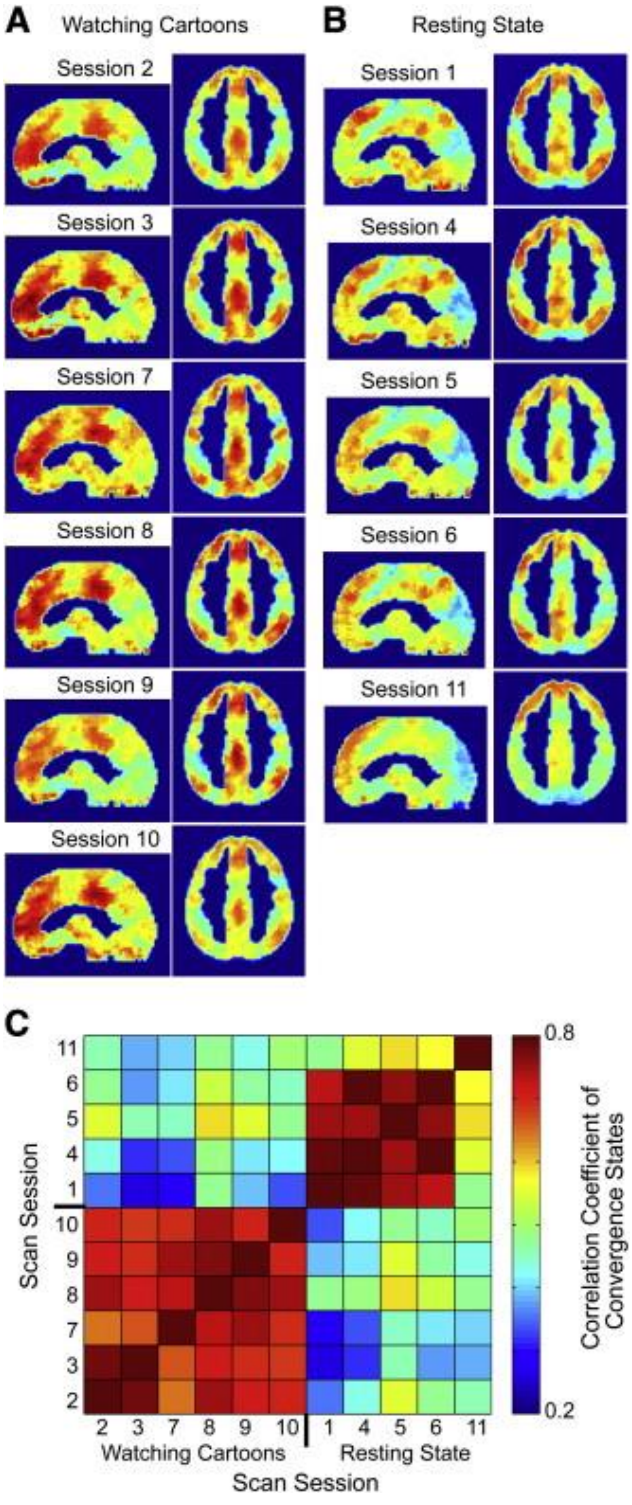
A
Watching Cartoons
Session 2
Session 3
Session 7
Session 8
Session 9
Session 10
B
Resting State
Session 1
Session 4
Session 5
Session 6
Session 11
C
Scan Session
11
6
5
4
1
10
9
8
7
3
2
2 3 7 8 9 10
Watching Cartoons
1 4 5 6 11
Resting State
Scan Session
0.8
0.2
Correlation Coefficient of Convergence States

connectivity-based whole brain simulations also showed reliable reproducibility at the single-subject level shown in Figure 6A. The convergence state for resting scans was reproducibly different from when the subject was watching cartoons. Moreover, the convergence state was reproducibly different for the individual subject than for the population. For example, the posterior cingulate node was more anterior for the individual than for the population, and the relative intensity of nodes reproducibly differed between the two task conditions as well as between the individual and population.

Metastable Intermediate Networks

In addition to final convergence to the default mode network, many of the simulations (n=949/5000) produced a metastable intermediate state characterized by a local minimum during iterations of the difference between steps, with eventual convergence to a different stable state. We used hierarchical clustering to categorize similarities between intermediate states, and observed six major clusters in the metastable configurations shown in Figure 7. The averaged outcomes for the metastable intermediates from each cluster exhibited spatial distributions with features of well characterized functional networks, including the visual (A,C), sensorimotor (D,E), dorsal attention (D,E), and salience-detection networks (F). In some cases, (D,E) intermediate states were a hybrid of two or more functional networks (sensorimotor, dorsal attention) of opposite polarity. In other cases, intermediate states resembled a portion of the

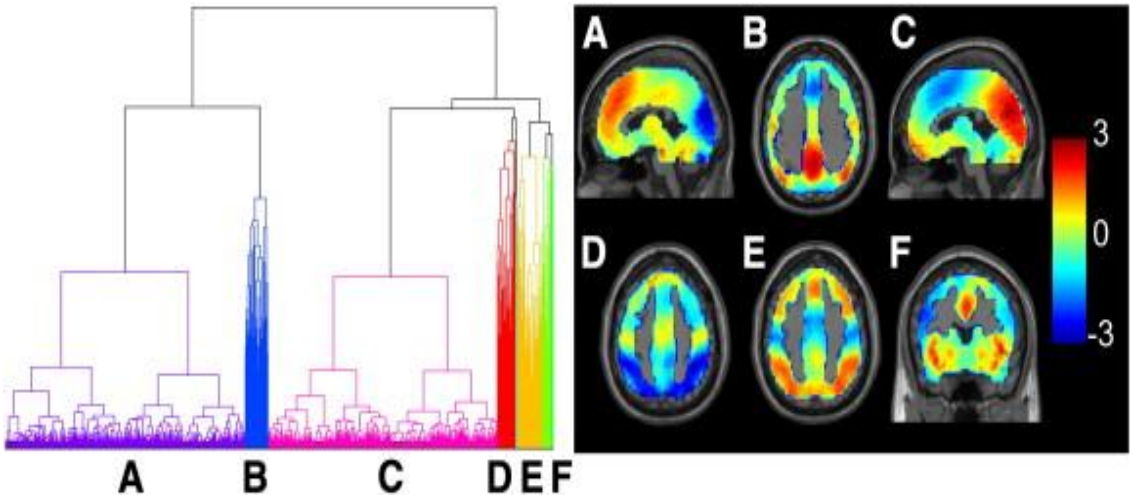

Figure 7: Clustering of metastable states. To the left is a dendrogram showing clustering of 949 simulations producing metastable states where a local minimum was seen during convergence. The images to the right show averages of the metastable states for each cluster, obtained at the time point where a local minimum was seen in the difference between steps of the simulation.

default mode network (B,C) in which one or more of the core nodes of the default mode network were absent.

In order to assess the effect of activity in any one brain region on convergence dynamics, we performed 7266 additional simulations, using activity corresponding to the functional correlation of each region in the brain with a seed region, and repeating for each region as the seed. We then measured the number of iterations needed to converge to the final convergence state within a tolerance of 0.05%. Seed ROIs that resulted in delayed convergence to the default mode network were located almost exclusively at the margins of the default mode network shown in Figure 8A and 8B. Sixteen of the 7266 simulations converged to the visual network. The seeds for which initial conditions converged to the visual network did not show any clustering or clear pattern in spatial distribution, but were scattered throughout the infratentorial and supratentorial brain. In converging to default mode network patterns of steady-state activity, dynamic iterations ultimately converge to one of two inverted mirror image states, one representing high activity in the default mode network, the other representing low relative activity in the default mode network. The determining factor for whether a steady-state outcome will represent high default mode versus low default mode activity is predicted by whether the initial starting conditions correspond more closely to correlation patterns for regions within the default mode network, or to correlation patterns for regions outside of the default mode network shown in Figure 8C.

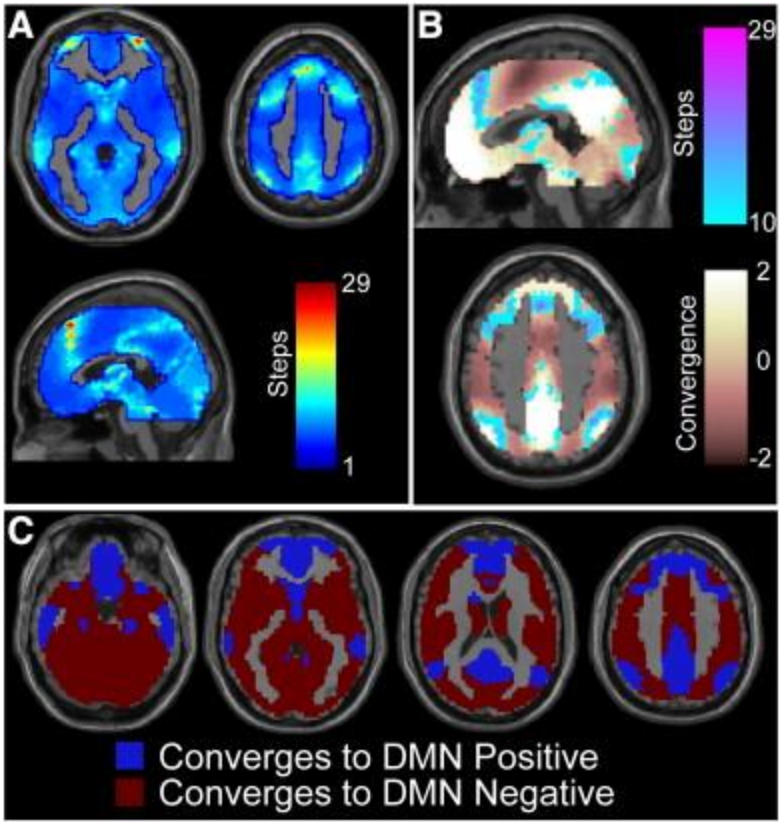

Figure 8: Steps to convergence, starting with the correlation network for each ROI. **A)** Color represents the iteration at which the simulation converged to within 0.05% of the final convergence state. Initial conditions for each ROI consisted of the normalized correlation across ROIs to the seed ROI. **B)** Initial conditions for which the simulation required 10 or more steps to converge, superimposed on the activity from the final default mode convergence state. **C)** Brain regions are shown in blue for which initial conditions with high activity only in this region resulted in convergence to a state with high default mode network activity. Initial conditions with high activity in regions in red converged to a state with low default mode network activity.

Discussion

Standard Map of Functional Connectivity

A population standard map of functional connectivity for the human brain underlies large scale imaging initiatives such as the NIH's Human Connectome Project and the INDI/NITRC 1000 Functional Connectome database. Our results confirm the reliability of datasets obtained from multiple sites converging to a reproducible whole brain functional connectivity map. By expressing the functional correlation matrix for each region as a linear combination of other regions, and iterating normalized brain activity over discrete time steps, we are able to obtain a convergent solution for the default mode network from a wide range of initial conditions. In greater than 99% of our simulations, the system converged to the default mode network (DMN), and in a large number of trials (n=949) passed through an intermediate metastable state before proceeding to its final convergence state.

Connectivity Hubs in the Human Brain

Regions of the posterior cingulate cortex, precuneus, medial prefrontal cortex, and medial temporal lobes have been classified as 'hubs' of structural and functional connectivity in anatomical studies of the human brain (42, 67-69). It is not surprising, then, that a dynamical system would converge toward a state in which the major hubs of connectivity were preferentially represented. This result is also consistent with the behavioral observation that during the resting

state, in which the BOLD data used for our simulations were obtained, the default mode network is consistently more active than during other cognitive tasks (6).

Convergence Outcomes in Whole Brain Model

In <1% of cases, the simulated brain converged to the visual network rather than the DMN, indicating that the functional connectivity relationships from the population likely exhibit not just metastability of multiple states, but actual multistability. Given the enriched density of high-participant hubs in the occipital lobe described by Hagman, et al. (69), this is also not surprising that the visual system would act as an attractor in some starting conditions. A possible implication of this finding is that the human brain is a multistable system driven toward one of several stability outcomes by a combination of environmental stimuli and previous state conditions. Future work may investigate the various conditions under which the system is driven toward DMN versus non-DMN convergence points.

The number of steps required for a given region's functional connectivity profile to converge to the DMN was prolonged for voxels at the margin of the default mode network and the attention control network. It has been previously shown that resting state functional connectivity can exhibit sharp transitions at areal boundaries, and that these transitions may serve to define functional domains (70). Our results indicate that convergence to a network is delayed more by activity at such boundaries than by activity in functionally opponent networks, such as activity within the attention control network.

For different sets of initial conditions simulating relative brain activity, dynamic iterations ultimately converge to one of two inverted mirror image states, one representing high activity in the default mode network, the other representing low relative activity in the default mode network (36, 37). The default mode network is balanced by relative activity in other brain regions and activity in any of those regions will lead to a state of decreased default mode activity when activity is iterated over time using connectivity-based evolution of brain activity. Among regions that converge to low default mode network activity, even regions that themselves are not directly anticorrelated with or functionally opponent with the default mode network are preferentially connected to regions that are, resulting in patterns of brain activity that over time result in stable default mode network suppression. In contrast, activity in regions associated with the default mode network will converge to a dynamically stable state with higher relative activity within the default mode network.

Representing Intrinsic Connectivity by Cholesky Decomposition

To obtain convergent results that showed the architecture of intrinsic connectivity networks, we had to express the functional correlations between brain regions as a linear combination of other regions rather than simple correlation coefficients between regions. Applying correlation coefficients without transformation to the same iteration led to convergence states that were a gradient from the front to back of the brain that appeared to overemphasize local connectivity. The Cholesky decomposition method we propose may allow greater

specificity in determining actual connections between brain regions, which may be useful for generating more accurate graph-theoretical representations of interregional connectivity (69, 71).

Comparison of Cholesky Decomposition to Partial Correlation Analysis

The Cholesky decomposition is a different approach to weighting brain connections than correlation-based methods. Instead of correlation or partial correlation, which express how synchronized brain regions are, the Cholesky approach directly evaluates how activity in one region may arise from a linear combination of other brain regions. Like partial correlation, it allows disentanglement of direct connections from connections to a shared input. But unlike partial correlation, instead of breaking down and losing long distance connections in a dense connectome with many closely related or overlapping nodes, the Cholesky decomposition preserves long-distance connections but with much greater specificity than seen using full correlation. Moreover, whereas partial correlation may be easily calculated when the correlation matrix is invertible, the Cholesky decomposition requires only a positive definite correlation matrix.

Model Limitations

Our results are drawn from averaging across a broad age range included in the subject sample. It is likely that different subject demographics may influence dynamical stability of intrinsic connectivity networks given known differences in functional connectivity across development (72, 73). It is also likely that the types and frequencies of metastable and multistable convergence points will vary across the lifespan according to the natural development of neural connectivity with age.

We also note that our model iterates normalized rather than absolute brain activity to constrain activity values to physiologically plausible levels. Exploring other types of normalization may better represent physiological mechanisms such as adaptation or other nonlinearities known to exist in the brain. Nevertheless, there is evidence that normalization mechanisms occur in the brain, wherein neural conductances are reduced by pooled neural activity from a population of neurons (74). Some form of normalization is certainly required given that energy constraints on the brain prohibit indefinitely additive circuitry, and blood flow to the brain is relatively constant over time, from which BOLD measurements are derived.

An additional limitation of our approach is that discrete steps in the simulation do not reflect explicit timing of interactions brain regions, and do not allow us to conjecture about transition times between initial conditions and convergence states, or temporal duration of metastable intermediate configurations. Undirected correlation measurements are also a simplified

paradigm for connectivity. In order to create more realistic whole brain simulations, improved methods are needed for modeling the asymmetries of effective connectivity between regions, including circuits such as corticostriatal projections known to contain one-way (non-reciprocal) connectivity. Further, a solution to the Cholesky decomposition requires a positive definite correlation matrix. Although the mean functional correlation matrix for the population we studied meets this requirement, it is possible that other study populations will not result in positive definite matrices. In such cases, other methods or extensions would be necessary to analyze the functional correlation matrix using alternative decomposition strategies, such as decomposition to a “best fit” triangular matrix.

Future Applications of Dynamical Whole Brain Modeling

In spite of these limitations, there are numerous possible applications for this approach to whole brain modeling. It is conceivable that various disease states may be typified by their variations in the multistability and metastability of large scale networks, given known differences in functional connectivity between patient populations (16-18, 75, 76). Methods for modeling stability of distributed brain networks may allow identification of relatively small subsets of nodes for which perturbation can affect brain network stability through control theory or other dynamical systems methods (77), and allow informed design of therapeutic strategies such as transcranial magnetic stimulation or deep brain stimulator placement. Changes in functional connectivity are known to exist with cognitive tasks (78), and examination of changes in convergence states with data obtained

during specific tasks may allow characterization of how stimulation may prime the brain for greater stability in different distributed networks. Lastly, there is potential to examine the normal course of brain development by examining changes in dynamical stability of brain networks with age and brain maturation. In short, methods that move beyond static functional correlation to examine dynamical network properties may provide additional characterization of brain networks and states relevant to behavioral and pathophysiological mechanisms.

Conclusions

Functional connectivity MRI (fcMRI) has become a widely used technique in recent years for measuring the static correlation of activity between cortical regions. Using a publicly available resting state dataset (n=961 subjects), we obtained high spatial-resolution maps of functional connectivity between a lattice of 7266 regions covering the gray matter. Average whole brain functional correlations were calculated, with high reproducibility within the dataset and across sites. Since correlation measures not only represent pairwise connectivity information, but also shared inputs from other brain regions, we approximate pairwise connection strength by representing each region as a linear combination of the others by performing a Cholesky decomposition of the pairwise correlation matrix. We then used this weighted connection strength between regions to iterate relative brain activity in discrete temporal steps, beginning both with random initial conditions, and with initial conditions reflecting intrinsic connectivity networks using each region as a seed. In whole brain simulations based on

weighted connectivity from healthy adult subjects (mean age 27.3), there was consistent convergence to one of two inverted states, one representing high activity in the default mode network, the other representing low relative activity in the default mode network. Metastable intermediate states in our simulation corresponded to combinations of characterized functional networks. Convergence to a final state was slowest for initial conditions on the borders of the default mode network.

By mathematically decomposing the functional correlations across 7,266 ROIs in the human brain, we are able to approximate the underlying weighted connectivity between gray matter regions. This approach is superior to existing analytical methods such as partial correlation analysis, in the sense that it preserves contributions from long range connectivity better than partial correlation analysis when large numbers of nodes are included in the model. The weighted connectivity can then be used in a whole brain dynamical model, demonstrating multistable convergence outcomes, with the default mode network showing greatest stability. This method is reproducible at a single-subject level of analysis, and is sensitive to changes in functional connectivity affected by task-specific dynamics. We also demonstrate metastable qualities of the human connectome, with intermediate configurations resembling well-characterized functional networks. The default mode network steady-state convergence outcomes are either reflective of high relative DMN activity or low relative DMN activity, contingent upon whether starting conditions for neural activity are correspondent to in-network or out-network connectivity patterns for the default

mode network. Finally, we demonstrate the borders between default mode network and attention control network are the slowest to converge to the default mode network.

CHAPTER 3

ALTERED RESTING FUNCTIONAL CONNECTIVITY OF EXPRESSIVE LANGUAGE REGIONS AFTER SPEED READING TRAINING[2]

Abstract

A goal of interventions designed to increase reading speed is to reduce the practice of articulating words in an individual's thoughts, or subvocalization. This practice may require redundant cognitive resources, slow reading speed, and detract from efficient transfer of written words to semantic understanding. It is unclear, however, whether exercises designed to promote faster reading speed generalize to cognitive function beyond the reading task itself. To investigate this possibility, we measured resting state functional connectivity in classical language regions before and after a course of cognitive exercise designed to increase reading speed in 9 healthy adolescent female volunteers (Table 1). We found significantly decreased correlation between left Broca Area and right Broca Homologue and between right Broca Homologue and right Wernicke Homologue in the resting state after the training period compared to

[2] Reprinted with permission. This is an Accepted Manuscript of an article published by Taylor & Francis in Journal of Clinical and Experimental Neuropsychology on 28 April 2014, available online: http://www.tandfonline.com.ezproxy.lib.utah.edu/doi/full/10.1080/13803395.2014.908825

before training. Differences in functional connectivity after training to left Broca Area showed a spatial distribution reflecting decreased correlation to memory-associated brain regions and increased correlation to auditory regions, that might be consistent with a hypothesis that such training may decrease subvocalization associated with semantic memory function during the resting state.

Introduction

The ability to read is a high-level cognitive capacity supported by the functional convergence of multiple lower-level sensory processes. As such, reading ability is considered a model system for exploring the emergence of higher order cognitive processes from their more evolutionarily basal building blocks (79, 80). The ability to engage written language (i.e., orthography) relies necessarily on basic visual processing systems that have evolved in the human brain for this purpose. Additionally, the refined primary sensory development of the human auditory system supports the phonographic engagement of spoken language. Successful integration of orthographic visual input and phonographic auditory data has been referred to as the *sine qua non* of the human ability to read (81). Unsurprisingly, canonical language regions along the perisylvian fissure (e.g., Broca and Wernicke Areas) have demonstrated a crucial role specifically in the convergence of orthographic and phonological processing that support reading ability (82-84).

Multiple studies have explored the plasticity of brain networks involved in reading performance, and the ability of these brain regions to adapt under short-

term training. In a study on pre-adolescent children with dyslexia, a two month interventional reading program showed fMRI-based activation changes that correlated with the degree of linguistic skill improvement (85). Similarly, a fourteen-day reading intervention program conducted for ten children with dyslexia demonstrated significant functional changes in regions associated with language tasks (86). A number of topically-related studies have likewise reported changes in activational patterns in the brain during reading tasks after interventional programs conducted across weeks to months (87-89).

In recent years, functional connectivity magnetic resonance imaging (fcMRI) has emerged within the neural imaging community as an effective metric of functional relationships in the human brain (3). Research in fcMRI has given a framework for understanding the large-scale architecture of human brain networks (4, 10). The majority of the studies published in the fcMRI literature take advantage of the fact that the strength of functional relationships across the brain are captured by the correlations in spontaneously occurring neural activity during a task-neutral state of wakeful rest. Because functional correlations are measured during a task-neutral resting state, they are considered to reflect the underlying structural connectivity (11). Further, changes in the functional connectivity assessed during a task-neutral state are therefore used to mark alterations in synchronized co-activation of brain regions, resultant from plasticity and adaptation of neural systems to external conditioning.

Despite a series of publications looking at changes in neural activity from reading intervention, there is a dearth of published studies that have explored

changes in the intrinsic connectivity in response to interventional reading training. Such studies are of interest, however, in their distinct contribution toward understanding brain plasticity from high-level considerations of structural-functional adaptations to task-based conditioning. In contrast to task-based data, which reflect regional adaptation and local neural efficiency, functional connectivity investigations provide an opportunity to explore changes in distributed connectivity that support learned behaviors, acquired skills, and habit formation.

As a test case for examining the effect of behavioral training on the functional architecture of networks involved in reading, we employed a speed reading training program aimed at altering the mechanisms for skilled reading. A core claim of speed reading proponents is that learned associations between orthographic and phonologic processing actually slow down the process of visual reading via subvocalization, the tendency of a reader to internally speak the words they are reading visually (90). In theory, such a tendency represents cognitive redundancy, in the sense that language content is transformed from visual cues into auditory cues by the reader, and then deciphered for meaning.

Consistent with this theoretical view, reduction or elimination of subvocalization in favor of direct semantic processing from visual cues, rather than semantically processing subvocalized phonological cues, would represent reduced cognitive load during the reading process, and allow reading to proceed at a faster rate. Because speed reading training provides a direct intervention for modulating a specific cognitive behavior, and additionally provides a framework

for expected brain regions involved in cognitive adaptation, it is a suitable paradigm for examining the relationships between behavioral training and underlying changes to functional neural architecture. We attempted to determine whether a course of training involving speed reading practice would be associated with detectable changes in functional connectivity in brain regions associated with language that generalized to a resting state, and not associated with merely the act of reading alone.

Methods

Participant Sample

To minimize heterogeneity of the sample, all participants were typically developing right-handed young female adolescents, ages 14-22. A total of 9 participants completed both initial and followup scan after performing the cognitive training exercises. Participants were recruited by posted flyers at an area high school. Reading proficiency was assessed using the Gray Oral Reading Tests (GORT-4) (91) at enrollment into the study. All subjects consented to participate in the study following informed consent under guidelines agreed upon by the University of Utah Institutional Review Board. An additional sample of 26 typically developing male participants was selected from an ongoing longitudinal study involving functional MRI connectivity. These data were obtained on the same scanner with the same protocol, pulse sequence, and same instructions to participants for resting state scanning, and are included for public release in 2014 as part of the Consortium for Reliability and

Reproducibility dataset from the International Neuroimaging Datasharing Initiative. For these subjects, age range was from 8 to 39 (mean 20.2 +/- 8.3 yrs). Individuals were scanned twice, at least 2 years apart (mean 928 days +/- 105 days, range 733 – 1187 days).

Cognitive Exercise Training

Subjects were instructed to participate in a 6-week intervention consisting of internet-based training (EyeQ Advantage, Salt Lake City). Before a repeat MRI scan, subjects were required to complete 12 modules designed to facilitate progressively faster reading speed and increased comprehension. Each training exercise lasted approximately 10 minutes, and most of the participants performed many of the modules multiple times, with engagement in the training 3-5 times weekly. Modules consisted of practice reading passages at slow, medium, and fast presentation speeds, as well as following with their eyes the presentation of geometric images placed at progressively faster speeds around a computer screen as an exercise in shifting visual attention. Each module consists of similar exercises performed in the same order. For the initial scan, subjects were naïve to any training, and performed their first module as the final sequence obtained during the first scan.

fMRI Acquisition

Images were acquired on Siemens 3 Tesla Trio scanner. The scanning protocol consisted of initial 1 mm isotropic MPRAGE acquisition for an anatomic

template. BOLD echoplanar images (TR= 2.0 s, TE = 28 ms, GRAPPA parallel acquisition with acceleration factor = 2, 40 slices at 3 mm slice thickness, 64 x 64 matrix) were obtained during the resting state, where subjects were instructed to "Keep your eyes open and relax. Remain awake and try to let thoughts pass through your mind without focusing on any particular mental activity." Prospective motion correction was performed during BOLD imaging with PACE sequence (Siemens, Erlangen). An 8-minute scan (240 volumes) was obtained for each subject. On the initial scan an additional fMRI sequence (7-minutes, 210 volumes) was obtained during performance of the first cognitive training exercise module. For both scans, an additional task-based sequence (4-minutes, 125 volumes) was obtained during presentation of a sentence completion visual language task. Details of this task have been presented previously (92). Briefly, a 20-second block paradigm alternated between periods of fixation on an isoluminant screen and periods where subjects read sentence fragments "He put the dishes in the _____" and covertly thought in their mind of a word to complete the sentence.

fMRI Preprocessing

Offline post-processing was performed in Matlab using SPM8 software. Post-processing pipeline has been previously reported (66, 93). Initial slice timing correction was performed to adjust for interleaved slice acquisition. Field map sequence was acquired for each subject for distortion correction, and all images were motion corrected using realign and unwarp procedure. BOLD iages were

coregistered to MPRAGE anatomic image sequence for each subject. All images were normalized to MNI template brain (T1.nii in SPM8), with manual inspection of appropriate normalization in all subjects.

For resting state scans of both the cognitive exercise subjects and 26 control subjects, we used a regression algorithm using time series from voxels in the facial soft tissues, CSF and white matter to correct for artifactual correlations in the BOLD data to correct for BOLD signal attributable to physiological noise such as heart rate and respiration, (38). No global signal regression was performed to avoid introducing artifactual anticorrelations in the data (39, 40).

Scalp and facial soft tissues, CSF and white matter regression was performed after automated gray matter, white matter, and CSF segmentation of each subject's MPRAGE image using SPM8. These segmented images were manually inspected to confirm appropriate identification of tissue components. The CSF time series for each subject was measured from the lateral ventricles. This was obtained from selecting voxels from the CSF segmented image for each subject within the bounding box defined by MNI coordinates: $-35 < x < 35$, $-60 < y < 30$, $0 < z < 30$. White matter time series for each subject were obtained from the mean time series of voxels within 2 regions of interest in the bilateral centrum semiovale (MNI coordinates: *left:* x=-27, y=-7, z=30; *right: x*=27,y=-7, z= 30, each ROI had 10-mm radius). Before extracting the white matter time series, an exclusive mask was performed with the gray matter segmented image from each subject to eliminate voxels containing gray matter. A soft tissue mask of the facial and scalp soft tissues was used as previously described (40). The mean

soft tissue, CSF and white matter time series were then used as regressors in a general linear model (glmfit.m in Matlab Statistics Toolbox) for the BOLD time series at each voxel in the brain, and the best fit was subtracted from the voxel's time series data, producing the signal-corrected time series images. Each voxel's time series was bandpass filtered with a frequency window of 0.001 Hz to 0.1 Hz (63) and linearly detrended to correct for scanner drift. No spatial smoothing was performed. Each frame was then inspected for significant motion using procedure reported by Power et al (30), and frames with DVARS or root-mean-square motion parameters > 0.2 were removed prior to analysis of connectivity results.

ROI Selection

Because the primary outcome of interest was the effect of functional connectivity in classical language regions, a 5 mm radius ROI was selected centered at MNI coordinates from the literature for left Broca Area and right Broca Homologue in the inferior frontal gyrus (left: x=-45, y=23, z=-2; right: x=36, y=24, z=-4) and left Wernicke Area and right Wernicke Homolgoue in the posterior superior temporal sulcus (left: x=-54, y=-44, z=4; right: left:-63,-36,3; right: 50,-25,-2) (92). Functional connectivity was measured before and after cognitive training for left Broca Area vs. right Broca Homologue, left Wernicke Area vs. right Wernicke Homologue, left Broca Area vs. left Wernicke Area, and right Broca Homologue vs. right Wernicke Homologue. Identical ROI's were extracted from each scan of the 26 longitudinal participants without cognitive exercise training.

Because differences in functional connectivity were found for Broca Area vs. Broca Homologue, and because an a priori hypothesis was formed that cognitive training would decrease subvocalization in participants, we performed an additional exploratory analysis of functional connectivity between left Broca Area and the rest of the brain's gray matter. 7266 ROIs were selected to form a lattice covering the gray matter as previously described (93, 94). The ROIs averaged 4.9 +/- 1.3 s.d. voxels in size for 3 mm isotropic voxels. For each subject, the preprocessed BOLD time series was averaged from the voxels in each of the 7266 ROIs, and functional correlation with the time series from the ROI containing left Broca Area coordinates was performed.

To more effectively accountt for inter-individual differences in precise position of language regions, visual language task data was processed using standard general linear model using SPM8, with activation t-statistic maps averaged between the pre-treatment and post-treatment scans for each subject. Activated clusters for bilateral Broca Area and Homologue and bilateral Wernicke Area and Homologue were obtained for each subject by identifying all voxels within 2 cm of above literature-based coordinates exhibiting $p<0.05$ activation, uncorrected voxelwise, within the region. In two subjects, no right Broca Homologue voxels met this threshold, and in one subject, no right Wernicke Homologue voxels met this threshold. For these individuals, 10 mm ROI's were selected surrounding the coordinates for right Broca Homologue or right Wernicke Homologue.

NeuroSynth Database

To assess the spatial distribution of functional connectivity differences associated with cognitive training, we attempted to determine whether changes in functional connectivity were associated with four cognitive domains: reading, memory (semantic), visual, and auditory function. For each case we obtained a mask of brain voxels associated with each function in the neuroimaging literature using the NeuroSynth database (95). For the search terms “reading,” “memory,” “auditory,” and “visual” we obtained reverse inference maps showing voxelwise specificity for the corresponding search terms in the literature, with false discovery rate $q<0.05$ for multiple comparison corrections. In these images, Z-scores were averaged for voxels in each of the 7266 ROIs for which they were nonzero, and spatial correlation was performed across regions between the Z-score for the search term and the T-statistic that functional connectivity of the region to left Broca Area differed between pre- and post-training scans. We were therefore testing whether differences in functional connectivity to left Broca Area were spatially localized to a particular cognitive domain.

Results

Resting state functional MRI images were obtained for each of 9 participants that completed cognitive training exercises before and after the training period. On the initial scan all subjects were naïve to the training software, and had not previously attempted a speed reading practice. On the followup scan, all participants had completed all 12 modules of the internet-based

software at least one time, and most subjects had performed the modules multiple times. All 9 of the participants exhibited increase in reading speed measured by the training software over the course of the modules. These increases are shown for each subject in Figure 9A, and were significant ($p=0.0021$).

Regions of interest containing literature coordinates and subject-specific activated voxels in a neighborhood surrounding these coordinates for left Broca Area and Wernicke Area, and the corresponding right hemispheric homologues were extracted for each subject both before and after training. Functional connectivity measurements were obtained as the Fisher-transformed correlation coefficient between the preprocessed time series of (1) Left Broca Area to right Broca Homologue, (2) Left Wernicke Area to right Wernicke Homologue, (3) Left Broca Area to Left Wernicke Area, and (4) right Broca Homologue to right Wernicke Homologue. Results are shown as a bar graph in Figure 9B for the activation-map derived clusters. There was a significant decrease in functional connectivity between left and right Broca Area and Homologue consistent with our hypothesis that subvocalization would be decreased following training and that functional connectivity would be decreased between expressive language regions ($p=0.017$, one-tailed t-test for literature-based coordinates, $p= 0.036$ for activation-map derived clusters shown in Figure 9B, one-tailed t-test). For activation-map derived clusters, there was also decreased functional connectivity between right Broca Homologue and right Wernicke Homologue after cognitive

Figure 9: **A)** Bar graphs show reading speed (words per minute) pre- versus post-training. (p=0.0021 for differences between reading speed pre- versus post-
(Figure 9 Continued) training). **B)** Bar graphs show mean functional connectivity across 9 participants, with error bars representing standard error of the mean. Results are shown for four region to region comparisons as indicated in the text. Functional connectivity from left Broca Area to right Broca Homologue was significantly lower (*) after cognitive training (p=0.036) as was connectivity between right Broca Homologue and right Wernicke homologue (p=0.046). **C)** Bar graphs show mean functional connectivity for healthy control subjects not participating in the reading training as indicated in the text, with error bars representing standard error of the mean. No significant differences are noted in functional connectivity across language areas indicated in the figure on baseline and repeat scans, separated by at least 2 years in 26 participants.

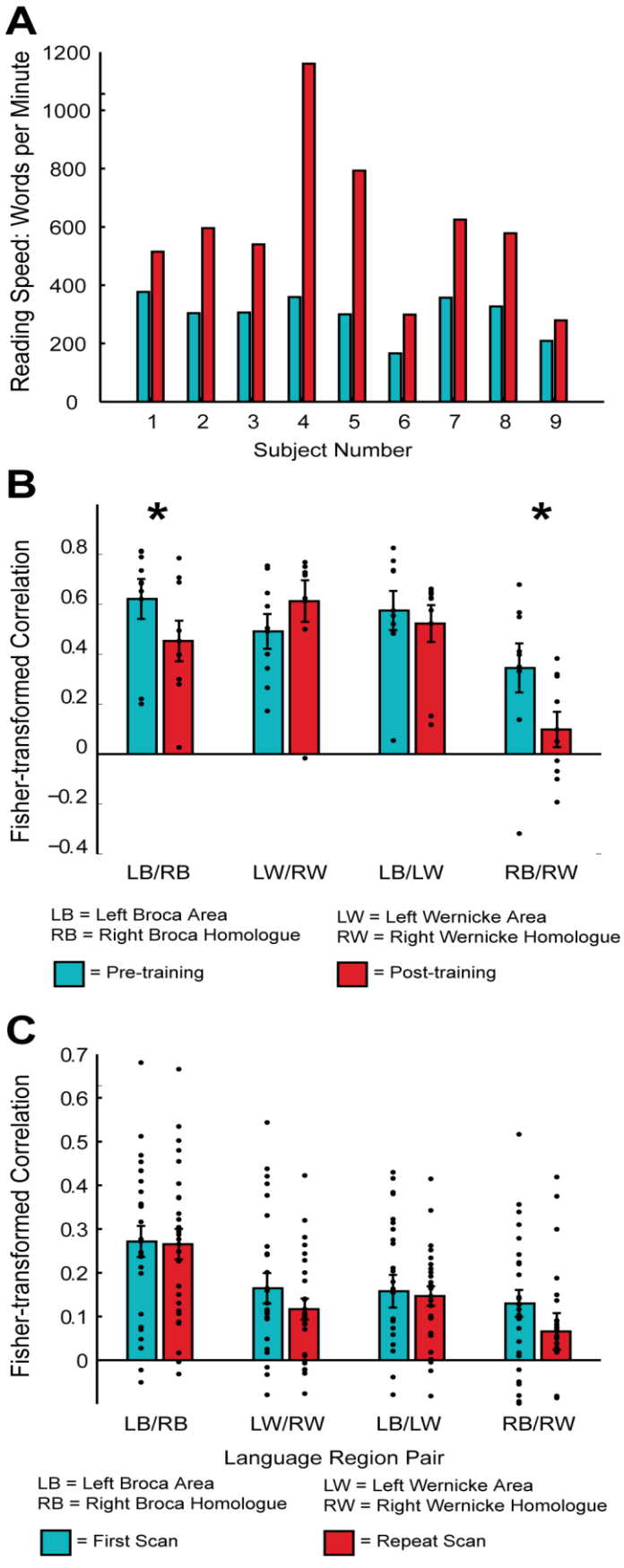
A
Reading Speed: Words per Minute
1200
1000
800
600
400
200
0
1 2 3 4 5 6 7 8 9
Subject Number
B
Fisher-transformed Correlation
0.8
0.6
0.4
0.2
0
−0.2
−0.4
*
*
LB/RB
LW/RW
LB/LW
RB/RW
LB = Left Broca Area
RB = Right Broca Homologue
LW = Left Wernicke Area
RW = Right Wernicke Homologue
= Pre-training
= Post-training
C
Fisher-transformed Correlation
0.7
0.6
0.5
0.4
0.3
0.2
0.1
0
LB/RB
LW/RW
LB/LW
RB/RW
Language Region Pair
LB = Left Broca Area
RB = Right Broca Homologue
LW = Left Wernicke Area
RW = Right Wernicke Homologue
= First Scan
= Repeat Scan

training (p= 0.046, one tailed t-test). No significant differences were detected for the other 2 comparisons.

In this sample, we did not observe significant relationships between functional connectivity differences and changes in reading speed recorded by the software over the course of training (left Broca Area to right Broca Homologue: r=-0.036, p=0.93; right Broca Homologue to right Wernicke Homologue: r=-0.089, p=0.83). No significant effect was observed between age and connectivity (left Broca Area to right Broca Homologue: r=-0.48, p=0.19; right Broca Homologue to right Wernicke Homologue: r=-0.26, p=0.49). A negative correlation was seen between baseline reading skill (GORT) and left Broca Area to right Broca Homologue (r=-0.86, p=0.12) but this was not statistically significant, possibly given the small sample size.

To evaluate whether this effect might be due to cognitive training or simply normal developmental processes, we compared the same metrics in the longitudinal sample without cognitive exercise training, using literature-derived coordinates. None of the four comparisons showed significant changes between the first and second scan in this cohort (left Broca Area to right Broca Homologue: p=0.90; left Wernicke Area to right Wernicke Homologue: 0.28; left Broca Area to left Wernicke Area: p=0.82; right Broca Homologue to right Wernicke Homologue, p=0.13) despite an even longer interval between scans (2 years) and larger sample size. Similarly, no correlation was found between age of the subjects across all 52 scans and any of the four connectivity metrics in this

sample. Individual subject values for each of these four connectivity metrics are shown in Figure 9C**.**

To further evaluate patterns of functional connectivity with left Broca Area, the expected primary locus for expressive language and putative region participating in subvocalization, we measured functional connectivity differences between this region and 7266 other ROIs covering the cortical and subcortical gray matter, and attempted to determine whether differences in functional connectivity to Broca Area aligned with a particular cognitive network as an exploratory analysis.

To accomplish this, we used the NeuroSynth database (95), consisting of inference maps to search terms in over 4000 studies in the neuroimaging literature. Specifically, we identified masks of brain regions significantly associated with the terms “auditory,” “visual,” “reading,” and “memory.” A significant reverse inference was indicative of a brain region specifically associated with these functions in the literature. For ROIs showing significant cognitive loading of each of the search terms, we compared T-statistics for differences in functional connectivity with left Broca Area before and after cognitive training, with the Z-score of loading for each of the search terms.

Results are shown in Figure 10. We found significant associations with two of the four search terms. For ROIs showing significant loading with the term “auditory” we found a correlation across ROIs that regions with higher loading of the term showed increased functional connectivity with left Broca Area after cognitive training ($r=0.2$, $p=6.0 * 10^{-13}$). For the term “memory” we found a

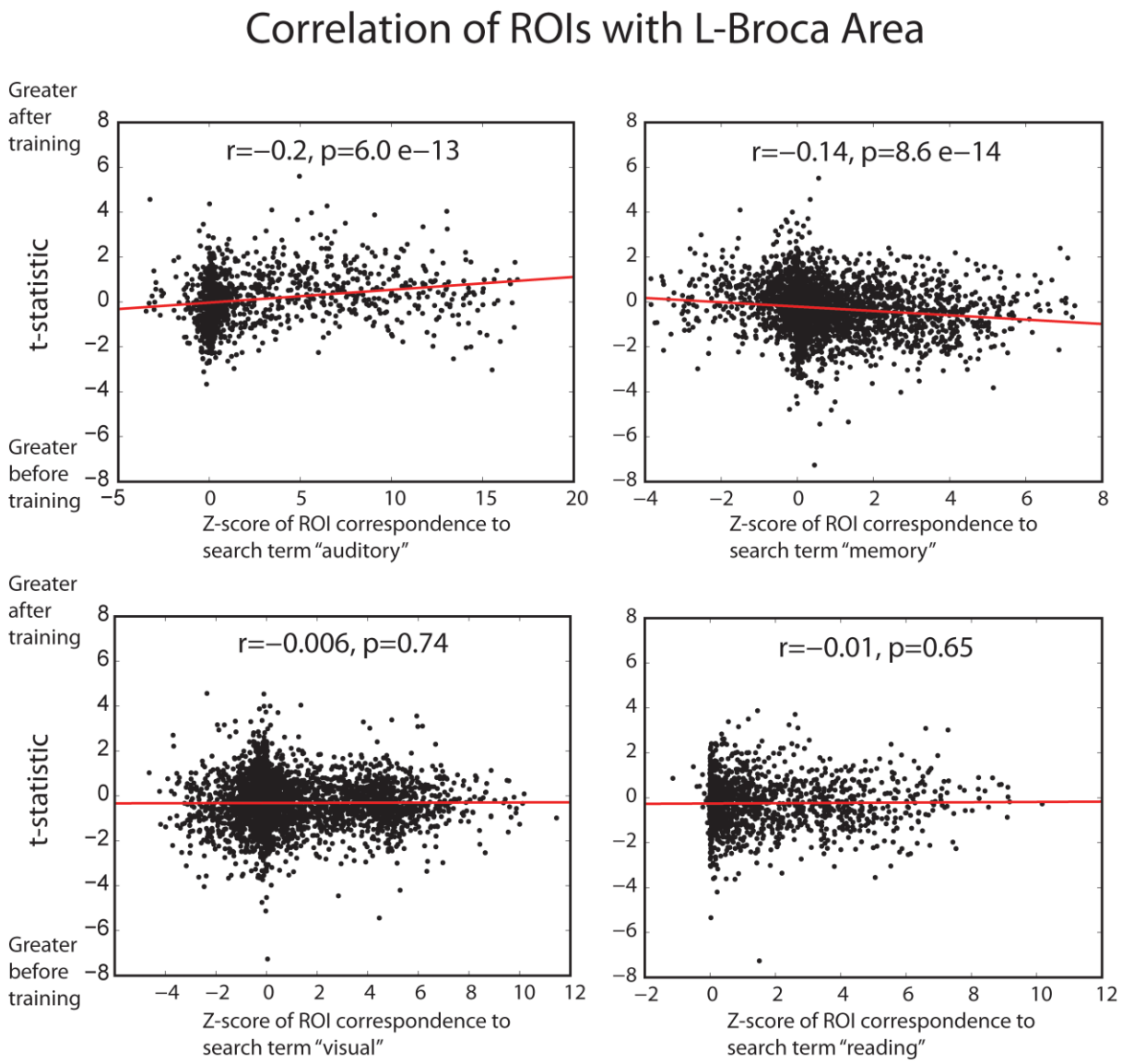

Figure 10**:** Scatterplots show spatial correlation of changes in functional connectivity to left Broca Area and loading to four specific terms in the neuroimaging literature. Masks were obtained for significant reverse inference to the terms "auditory," "memory," "visual," and "reading" in the NeuroSynth database, and Z-score for significant loading to each of these terms is compared to T-statistic for change in functional connectivity to left Broca Area across gray matter regions within the mask.

negative correlation between higher loading of the term and increased functional connectivity with left Broca Area after cognitive training across ROIs ($r = -0.14$, $p=8.6 * 10^{-14}$). The other two search terms showed no correlation between loading for the search terms in the literature and changes in functional connectivity to left Broca Area ("visual": r=-.0006, p=0.74; "reading": r=-0.01, p=0.65).

Images showing the spatial distribution of the "auditory" and "memory" masks as well as regions showing greatest changes in functional connectivity to left Broca Area before and after cognitive training are illustrated in Figure 11. The regions showing greatest differences in functional connectivity are closely aligned to "auditory" and "memory" networks, with greater functional connectivity to auditory regions after training, and relatively greater connectivity to memory regions before training. While the absolute differences in functional connectivity to left Broca Area do not survive multiple comparison corrections given the modest sample of 9 subjects (Figure 11A**)** is thresholded at $p<0.05$, uncorrected for display, the spatial distribution of changes is correlated to specific cognitive networks. Reverse inference in the NeuroSynth database for the terms "auditory" and "memory" demonstrate overlapping regional correspondences to areas of functional connectivity changes across subjects.

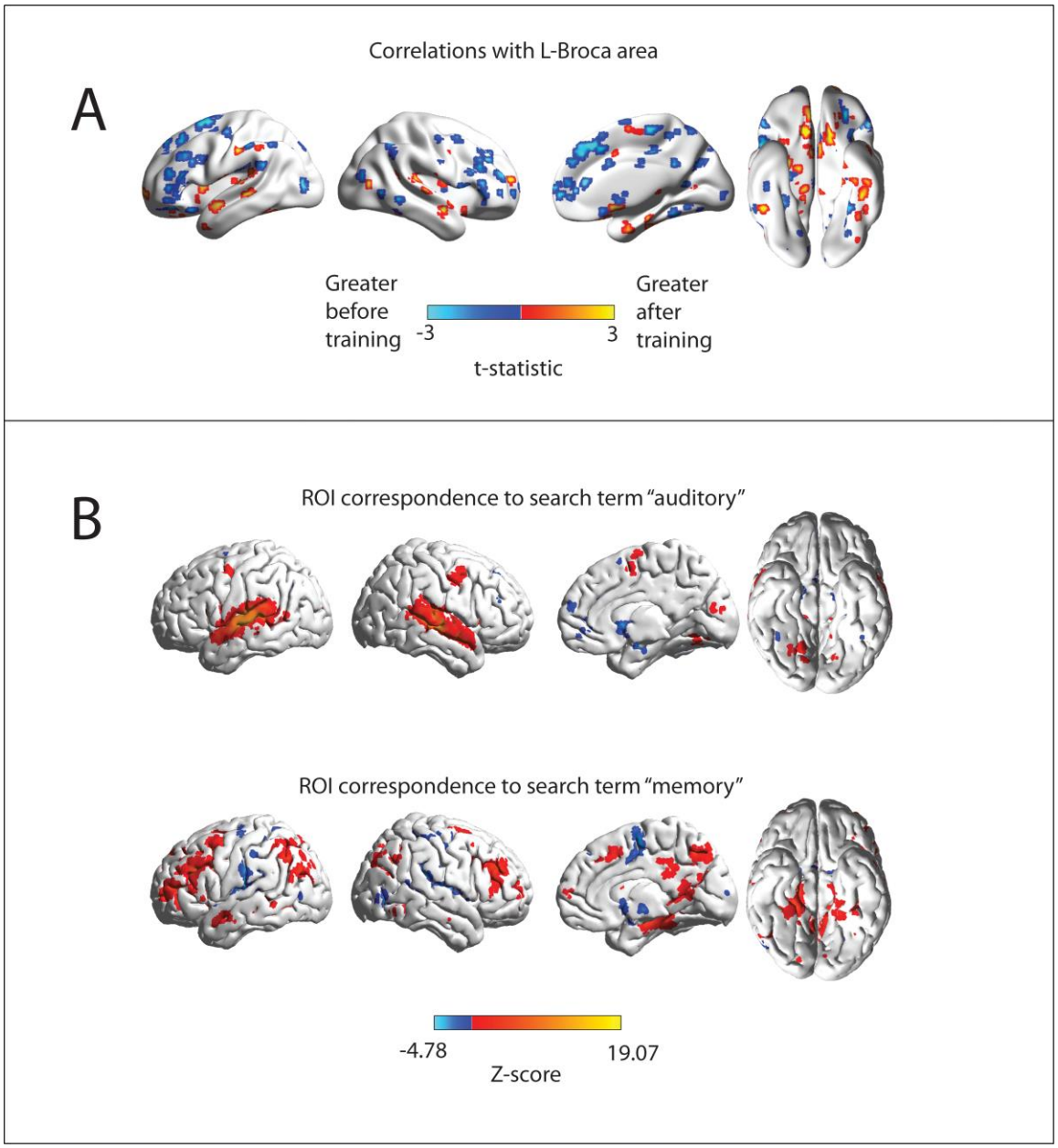

Figure 11**:** Spatial distribution of changes in functional connectivity to left Broca Area. **A)** Changes in functional connectivity after vs. before cognitive training of 7266 ROIs covering the gray matter to left Broca Area. Colored ROIs show regions that exhibited differential functional connectivity, thresholded at $p<0.05$, uncorrected, for display. **B)** Voxels showing significant reverse inference to the terms "auditory" and "memory" in the neuroimaging literature from the NeuroSynth database. Color scale represents Z-score for loading of the respective terms at each voxel, corrected for multiple comparisons with False Discovery Rate $q<0.05$.

Discussion

We demonstrate in a small cohort of adolescent female volunteers that a brief period of cognitive speed reading training results in resting state functional connectivity changes between left Broca Area and right Broca Homologue, independent of any task being performed. This might be consistent with, though not definitive for, a decrease in subvocalization during the resting state paradigm. Additionally, subtle changes in functional connectivity to left Broca Area show close alignment with cognitive networks underlying auditory and semantic memory function, with trends toward relatively decreased functional connectivity between Broca Area and memory-associated brain regions after training, and relatively increased connectivity between Broca Area and auditory-associated brain regions after training. This would be consistent with a hypothesis that function of Broca Area becomes more synchronized or associated with auditory function and less synchronized with memory function after training, possibly representing decreased subvocalization of semantic content during the resting state.

Although decreasing subvocalization is a common goal of reading proficiency training, the literature regarding brain activation changes associated with subvocalization is relatively sparse. In one early study, a task-based design required subjects to subvocalize words in a block design, with associated activation of left Broca Area (96). A unifying concept underlying function in Broca Area has been the association with speech or word generation and articulatory planning (97). Data from transcranial magnetic stimulation experiments has also

found that Broca Area was associated with excitability of the motor system underlying speech production (98). Inferior frontal gyrus, but also posterior cingulate and superior frontal gyrus activation have also been demonstrated in ERP and fMRI studies of mechanisms of subvocalization and semantic selection (99), Functional MRI during subvocal auditory rehearsal activated predominantly Broca Area in the left lateralized inferior frontal gyrus (100). It is likely that subvocalization may represent a process that spans from speech generation in inferior frontal gyrus to premotor areas and ultimately motor cortex with progressive vocalization of sounds.

How subvocalization might be reflected within functional connectivity is much less clear. Yet recent developments in brain network architecture have reinforced that synchrony of brain regions is a reliable metric of co-activation and co-localized function (3). In language processing in particular, engagement of progressively more difficult language tasks involves increased recruitment of right hemispheric language region homologues, and left dominance decreases systematically with activation threshold (101). Increased connectivity of bilateral Broca Area and between right Broca Area and Broca Homologue seen in our results with reading speed training designed to decrease subvocalization may indicate that increased synchrony and recruitment of inferior frontal gyri may be associated with changing patterns of subvocalization or engagement of the speech generation system during wakeful rest.

We hypothesized that Broca Area might be more active or more integrated with other language regions when individuals were articulating words they were

reading. If activity in Broca's area became more synchronized with auditory cortex and less synchronized with semantic memory regions with training, this would suggest reduced coactivation of articulatory planning and expressive language construction with reading comprehension and memory retrieval. In other words, Broca Area would become more aligned with auditory processing and less aligned or synchronized with memory and semantic processing regions engaged in comprehension. Although the changes in connectivity to left Broca Area are small, it is striking the degree to which these changes recapitulate precisely the spatial distribution of known auditory vs. memory networks. Future studies are needed to explore whether other quantification techniques of subvocalization (such as electromyography) will confirm activation of speech generation and premotor regions and whether functional connectivity may serve as a metric of subvocalization for following reading practice interventions.

A wealth of functional imaging literature from the past twenty years has pieced together a relatively fine-grained portrait of orthographic language processing. Most basically, the processes by which an individual learns to translate visual cues into semantic meaning involve functionally integrating visual attention regions and high-order language areas clustered around the left temporal lobe. Coactivation of homologous regions from the right hemisphere are observed in cognitively demanding language conditions or altered prosody or emotional content. This corresponds to a pattern observed across numerous tasks wherein contra-lateral recruitment of regions are observed for neurally demanding functions (102-104). The bottom-up construction of primary visual

cues into linguistic content is complemented by top-down phonological responses. This top-down contribution reinforces the end goal of appropriate semantic interpretation (105, 106). In skilled readers, the top-down phonological contributions to semantic processing are automated (107, 108).

A specific goal of the speed reading intervention applied in this study is to disassociate the visual input of orthographic word representations from internalized voicing and subvocalization of the text while it is being read. This hypothesis is consistent with our neuroimaging results, in that expressive language regions most associated with subvocalization appear to show more focused correlation to auditory regions associated with spoken language, but not with higher-order semantic or memory function associated with internal narrative or dialogue (109).

At the basic sensory level, the neural processes wherein visual input is converted to phonology can be parsed into at least three distinct pathways: sublexical, lexical, and semantic pathways (110). As such, the cognitive strategies for completing the same gross task (i.e., converting written language cues into phonology) demonstrate a significant amount of intersubject variability, since multiple strategic pathways are capable of accomplishing the same outcome. In spite of variability in cognitive strategy and neural pathways involved in reading, the commonality of the training task translates into a common focal point for the intervention: disassociating subvocalization of phonemes from their orthographic representations. As such, the observed reduction of functional

correlation strength between regions involved in expressive speech fit into an expected neurological model for changes due to the interventional training.

While the results indicating that functional connectivity changes can be seen even in a resting state may indicate generalization of training beyond reading function, several study limitations suggest additional study is warranted to understand the effects of cognitive exercise training. First, the study sample is modest, limiting statistical power of the functional connectivity changes that can be discriminated. The spatial relationship with the auditory and memory networks indicates only that to the extent functional connectivity changes are present, they are closely aligned with these networks. Nevertheless, a definitive whole-brain characterization of functional connectivity alterations that could survive rigorous multiple comparison corrections would likely require a much larger cohort. Additionally, there must remain tentativity about the interpretation of functional connectivity changes involving Broca Area and subvocalization, given uncertainty about the precise neural mechanisms of subvocalization and alternate possible hypotheses about changes in functional connectivity, given that functional connectivity does not produce unambiguous interpretations of neural processes. The observed differences in functional connectivity, however, are encouraging in their consistency with hypothesized language function and the anticipated effects of cognitive training.

It is possible that functional connectivity changes seen could represent developmental effects rather than cognitive training. To test this possibility, we included longitudinal data from an additional cohort spanning the age range of

our cognitive exercise subjects. No significant changes were seen in functional connectivity of classical language regions for this cohort, nor was there any relationship between age and connectivity for these regions. Nevertheless, these subjects were male, and the cognitive exercise subjects were female, so a gender-specific effect is not tested. Moreover, if developmental effects were specific to a very narrow age range in late adolescence, this might not be seen in the cohort spanning a larger age range (8-39).

Additional work would be required to demonstrate the durability and temporal evolution of changes in functional connectivity during reading interventions. It is unknown how much training is required to effect such changes, or how this might correspond to reading or cognitive performance. It has also been observed that Broca Area exhibits heterogeneity of function with overlapping regions processing phonology, syntax, and semantics, and a more detailed portrait of the functional connectivity of Broca Area will likely require higher-resolution discrimination of Broca complex subregions (111).

These results may inform future studies of reading interventions by focusing on the role of subvocalization and associated changes in functional connectivity with expressive language areas. Additional measurement strategies for quantifying subvocalization that are amenable to the MRI environment would be helpful for confirming the role of subvocalization in cognitive training. Further work will also be needed to establish the cognitive consequences of reduced subvocalization beyond reading and whether such training may contribute to enhanced cognitive function in attention, memory, or other domains.

CHAPTER 4

TYPICALITY AND DYNAMICAL STABILITY OF FUNCTIONAL CONNECTIVITY PREDICTS COGNITIVE ABILITY AND PROSOCIALITY

Abstract

Resting state functional connectivity MRI is a leading approach to characterize healthy and pathological brain function. Significant strides have been made to understand patterns of whole brain architecture across cortical and subcortical functional networks. The NIH Human Connectome Project (HCP) includes rich behavioral metrics for each participant, and the HCP 500 subject data release presents an unprecedented opportunity to quantify and model the relationships between human brain function and human behavior on a large scale. We present a novel multivariate correlation map for functional connectivity and behavioral metrics across 475 healthy participants using spectral decomposition to characterize eigennetworks at group mean and single-subject levels. We also present an approach to dynamical stability and metastability of functional connectivity at the individual-subject level. We find significant correlations between the typicality (similarity to group mean) of principal components of functional connectivity and cognitive ability. Moreover, we find

that greater dynamical stability of principal components resembling the default mode network are significantly correlated with prosociality metrics across individuals.

Significance

The Human Connectome Project 500 (HCP500) dataset provides unprecedented opportunity for large-sample, high-quality functional connectivity evaluation of personality and behavioral metrics in individual subjects of a typically-developing cohort. Defining biomarkers in a typically-developing population allows determination of canonical variants of human behavior that can be applicable to any neuropsychological and psychiatric disease population for which there is an adequate sample size to examine. We additionally present a method for dynamical evaluation of brain network stability. A dynamical stability assessment for attractor kinetics of brain networks (94) is applied to modern functional connectivity data, wherein extended imaging time per subject allows the opportunity for characterization of brain network stability, metastability, and their relation to behavior in individual subjects.

Introduction

Resting state functional connectivity maps the architecture of synchronized spontaneous fluctuations in neural activity. The resultant networks of functionally correlated regions comprise canonical networks of brain regions that show temporal coactivation (2-4, 10). Task-based fMRI experiments, years

before RSFC was developed, corroborate the existence of large-scale distributed networks with specific roles in supporting cognition (12). Task-based designs have constituted a wide range of experimental conditions, including facets of primary sensory perception, motor planning and execution, language processing, directed attention, and social reasoning (112).

The NIH-sponsored Human Connectome Project has used advances in fMRI acquisition and a standardized battery of behavioral metrics to create a detailed, publicly available research and clinical dataset for neurocognitive integration (113-119). Functional connectivity networks continue to be explored as potential sources for biomarkers in distinguishing single-subject characteristics relevant to disease pathophysiology and interindividual variations in cognition, and the Human Connectome Project dataset represents a unique dataset for characterizing the interrelationship of behavior and brain connectivity.

Individual behavioral metrics have been correlated with interindividual differences in brain networks identified using independent component analysis, yielding numerous significant relationships between specific cognitive performance differences and synchrony of ICA-defined brain regions (120). Additional biomarkers for the neurophysiology of disease are derived from principal component analysis of functional connectivity data, including information about dynamics and stability of functional configurations (14). While ICA yields valuable information about localization of spatially discrete network hubs (121), PCA offers other potential advantages. Components obtained are ranked with respect to the contribution of variance explained by the component (122), so that

components with highest eigenvalues may represent compact information about high-yield interindividual differences. Moreover, principal components represent configurations of a system, which show relative dynamic stability (94, 123), a feature that may be of interest in cognitive processes requiring sustained activity within a neural network. In this report, we describe relationships among principal components of functional connectivity and dominant modes of behavioral variation across individuals, with emphasis on functional connectivity patterns that may relate to dynamical stability of brain networks.

Results

Resting State Functional Connectivity

Functional connectivity was calculated between 361 pairs of cortical and subcortical gray matter regions of interest (ROI) for 475 subjects released with the Human Connectome Project dataset, resulting in a 361 x 361 matrix of Fisher-transformed correlation coefficients for each subject and for group mean functional connectivity. Principal component analysis of the group mean connectivity matrix yielded eigennetworks (ENs) that showed correspondence to canonical functional network architecture (Figure 12A). ENs from group-level analysis correspond to sensory and motor cortices (EN1, sensorimotor, auditory, and visual), default mode network (EN2), dorsal attention network (EN3,5), visual cortex (EN4), and permutations of hubs from known functional network architecture (EN 6-10). EN7 shows a pattern with strong lateralization of association cortex.

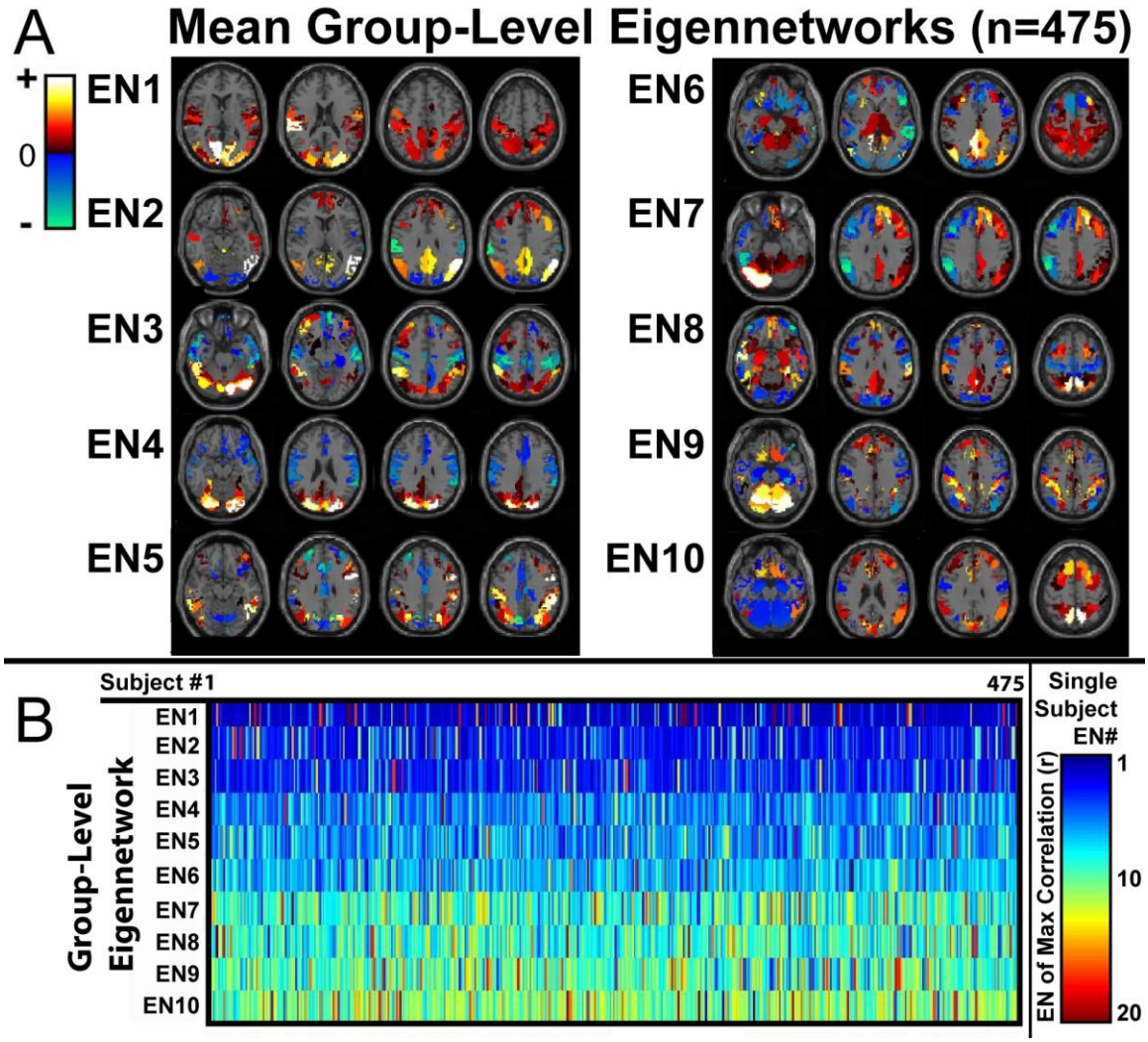

Figure 12: Principal components (eigennetworks) of functional connectivity for group-averaged and individual subject functional connectivity. A) The first ten principal components are shown from group-averaged functional connectivity between pairs of 361 brain regions. Both positive and negative features are shown for each component. B) Correspondence of most homologous single-subject principal components to group principal components are shown for 475 subjects.

When eigennetworks are extracted from connectivity matrices for each of the 475 individual participants, correspondence of group-level to subject-level ENs is greatest for EN1, with increased network heterogeneity across the population inversely related to network eigenvalues, i.e., EN rank (Figure 12B), but with relatively similar EN ordering across subjects through at least the first ten eigennetworks.

Behavioral Clusters

Behavioral measurements across 475 healthy control participants cluster into ten core features, labeled social support, negative affect, intelligence, executive function, delay discounting, positive affect, memory, prosociality, conscientiousness, and attention (Figure 13), based on the weightings of behavioral metrics associated with each factor.

Behavior/Connectivity Correlation

Relative scores for each behavioral component in each subject were correlated with subject-level eigenvalues corresponding to the subject-level eigennetwork best matching each of the first ten group-level eigennetworks. The behavioral component most associated with metrics of intelligence (progressive matrices, picture vocabulary, reading decoding, list sorting) in healthy control subjects is predicted by the eigenvalues for subject to group best-matched ENs 7, 8, 9, and 10, with a positive relationship between relative score on the intelligence factor and eigenvalues for each of the four networks (EN7,

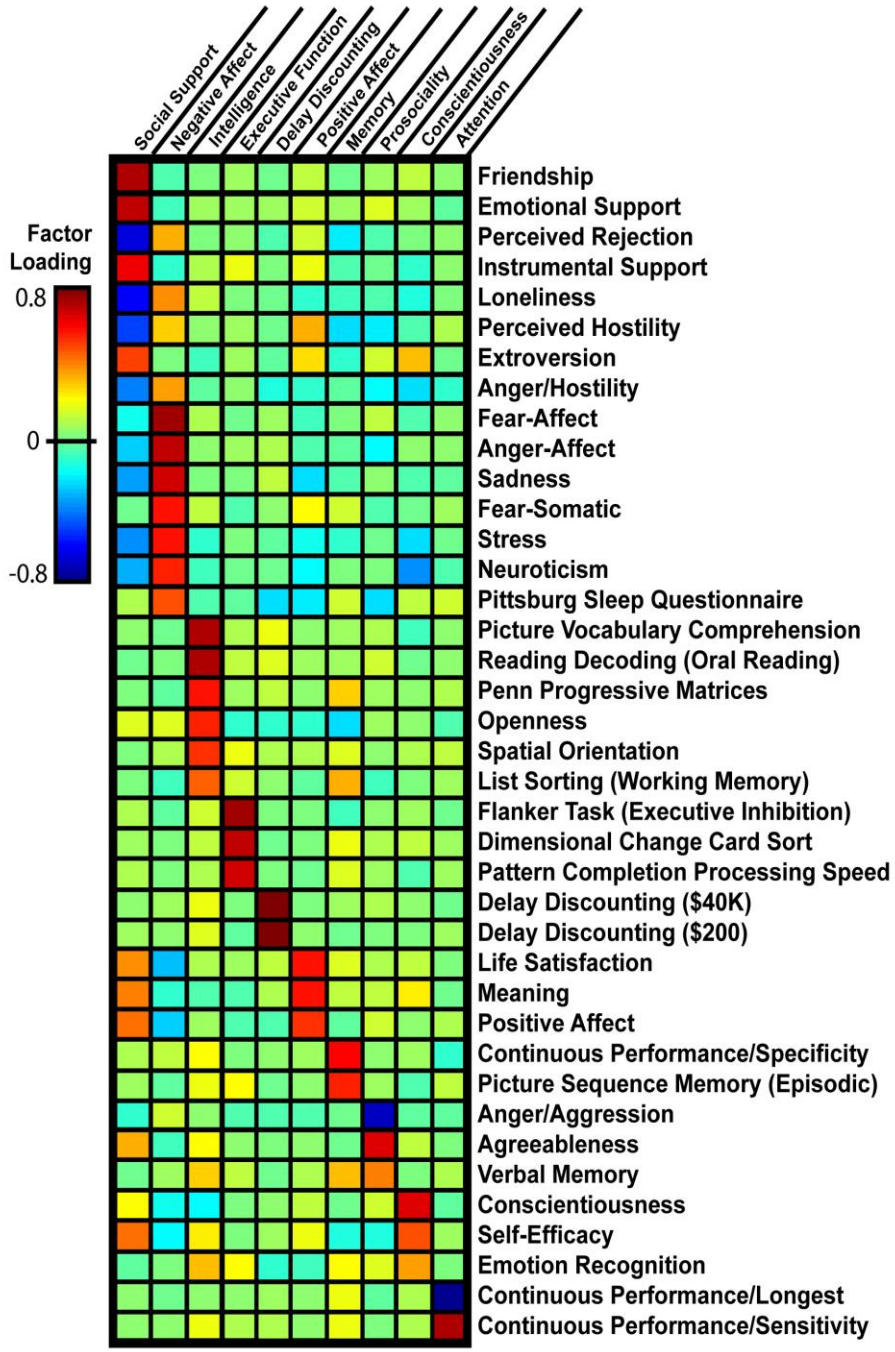

Figure 13: Weighting of behavioral metrics in 10 clusters. 39 metrics were selected for evaluation and separated into 10 clusters using principal component analysis with orthogonal rotation. Relative weightings for each metric in each cluster are indicated by color.

$p=2.26x10^{-4}$; EN8, $p=1.87x10^{-4}$; EN9, $p=1.06x10^{-4}$; EN10, $p=1.49x10^{-4}$ (Figure 14A). intelligence factor and eigenvalues for each of the four networks (EN7, $p=2.26x10^{-4}$; EN8, $p=1.87x10^{-4}$; EN9, $p=1.06x10^{-4}$; EN10, $p=1.49x10^{-4}$ (Figure 14A).

To evaluate for behavioral factors associated with social and emotive function, eigennetwork 2, which best recapitulates the architecture of the default mode network, was chosen for further evaluation given the homology of the default mode network and brain regions involved in social function (124). When evaluating typicality of subject-level eigennetworks (how well group-level EN correspond to matching subject-level eigennetworks), individuals' prosociality factor (low anger/aggression, high agreeableness) is significantly correlated with typicality of the subject's default mode network ($p=1.88x10^{-3}$, Figure 14B).

Dynamical Simulations

Whole brain simulations beginning with activity in one region and iterating brain activity stepwise in time using group-averaged functional connectivity between regions converged to the default mode network regardless of in which region the simulation began. In addition, simulations passed through transiently stable intermediate states, visualized in both line graphs and pseudocolor plots Single-subject simulations using individuals' functional connectivity matrices to model stepwise progression of brain activity show similar transiently stable intermediate configurations, with variations across subjects in key parameters.

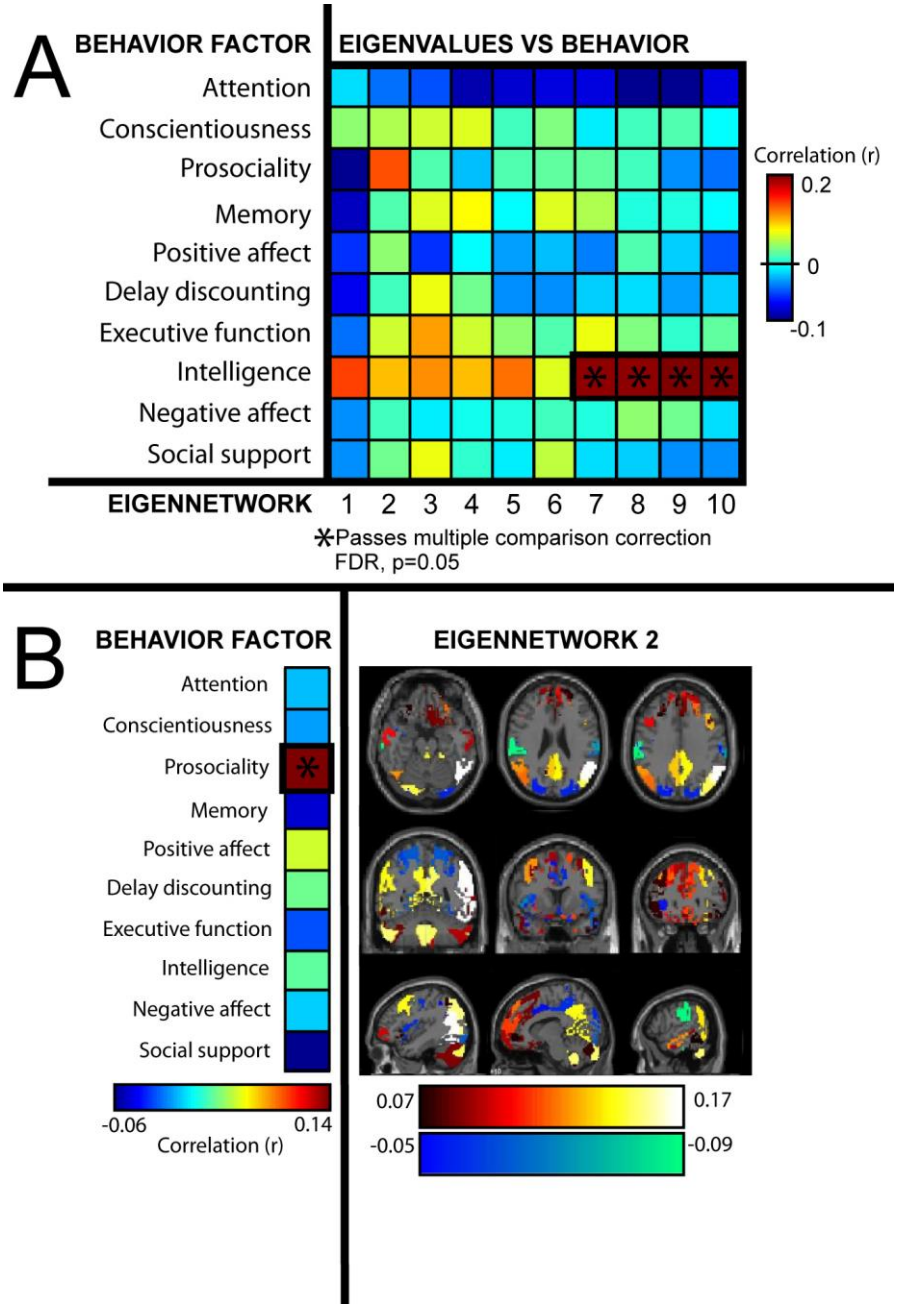

Figure 14: Correlation of principal components of functional connectivity to behavioral clusters across subjects. **A)** Spearman correlation coefficient across subjects of behavioral scores for each cluster and eigenvalues for eigennetworks most homologous to each group-level eigennetwork. **B)** Typicality of eigennetwork 2 was assessed by the spatial correlation between group level eigennetwork 2 with the single-subject eigennetwork with highest homology. This typicality showed significant correlation to behavioral prosociality scores across subjects.

as local minima in the sum of intensity fluctuations for all regions shown in Figure 15. The total number of local minima across all simulations, the minimum number of steps in the simulation to reach final convergence, and the correlation between individual subjects' final convergence patterns compared to mean group-level final convergence pattern were correlated with behavioral metrics across subjects, shown in Figure 16.

The average minimum number of steps for individual subjects' simulated brain activity to converge to final stability is positively correlated with conscientiousness, i.e., slower convergence to a global stable state predicts higher conscientiousness in behavioral domains ($p=7.11x10^{-3}$). Also, similarity of single-subject final convergence state to mean group-level final convergence is positively predictive of prosociality for the individual ($p=3.92x10^{-6}$).

Discussion

Using principal component analysis to decompose resting-state functional connectivity matrices, we examined principal components (eigennetworks) with the largest eigenvalues, comprising the greatest variance of group- and single-subject level functional connectivity. The most consistent eigennetworks from individual to individual across a sample of 475 healthy adults correspond to those with the largest eigenvalues in group-level eigennetwork analysis. Behavioral data from the 475 study participants clustered into ten categories of behavioral

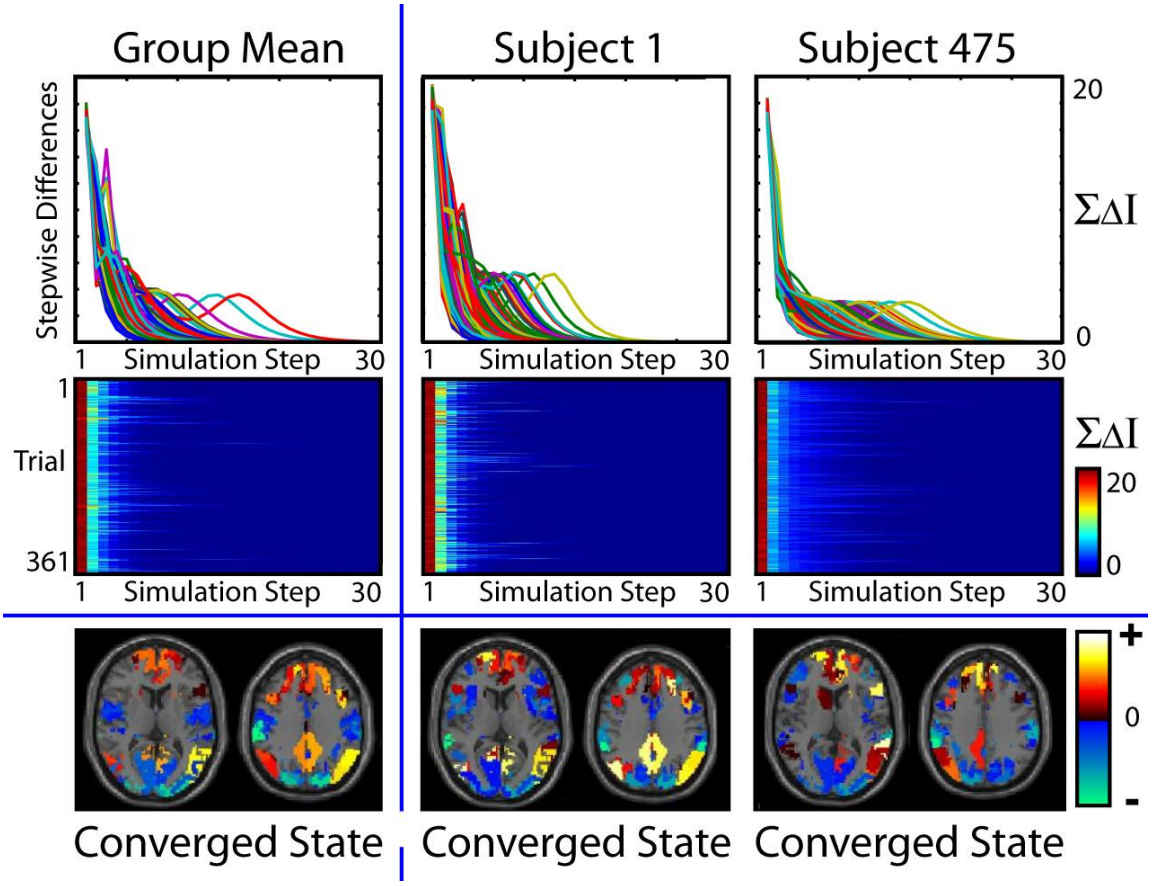

Figure 15: Convergence to the default mode network in dynamical simulations. Top row: Stepwise difference in mean intensity for iterated brain activity beginning in a single region. Each trace shows simulation beginning in a different region. Simulation from group mean functional connectivity is shown on the left and two individual subjects are shown to the right. Middle Row: Pseudocolor plot shows mean change in intensity for each step in simulations beginning with activity in each of the 361 regions. Bottom Row: Spatial pattern of the final convergence state. This was invariant for each subject, regardless of in which region the simulation began.

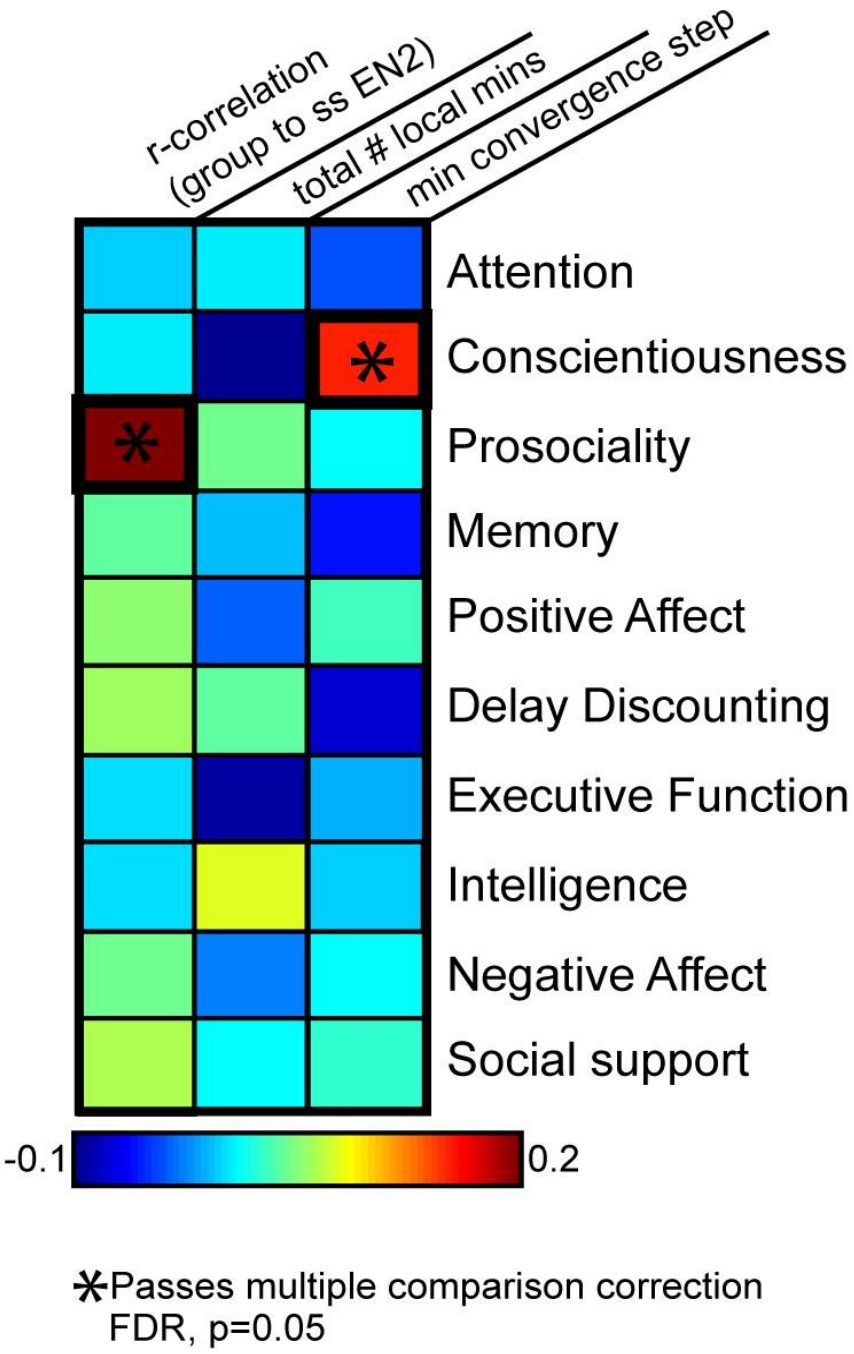

Figure 16: Correlation of simulation parameters to behavioral scores is shown. The first column shows correlation of behavioral scores to spatial homology of the single-subject convergence state to the group-level convergence state. The second and third columns show the total number of local minima for 361 simulations, and the average minimal step needed to converge for the simulations. Color scale shows spearman correlation coefficient.

features: social support, negative affect, intelligence, executive function, delay discounting, positive affect, memory, prosociality, conscientiousness, and attention. Several domains of behavior correlated significantly with features of principal components of functional connectivity data and simulated dynamical functional connectivity.

Cognitive performance (intelligence) across 475 subjects is significantly correlated with the eigenvalue of four of the ten eigennetworks, indicating that the degree to which highest-ordered group-level components are present in the subject's principal components reflect cognitive performance on behavioral tasks. Prosociality across individuals is significantly correlated with the closeness of fit between individuals' EN2 and group-mean EN2. Because group-mean EN2 represents the default mode network identified in traditional ICA of RSFC, we assert that prosociality in a healthy control population is predicted by the typicality of an individuals' default mode network, or similarity of the network to the group-averaged default mode network. It is notable that prosociality is not predicted by strength of DMN activity reflected in EN2's eigenvalue. Only the coherence to group-mean architecture and not variations in EN2's weighted contribution to functional connectivity predicted prosocial behavior. Simulated dynamic activity of individual subjects' brains reveal functional markers for conscientiousness. Conscientiousness in individual behavior is inversely predicted by how quickly individual subjects' simulated brains converge to steady-state default mode network architecture. In other words, the longer it

takes a subjects' brain to converge to a final default mode network steady-state, the higher the individual scores on behavioral measures of conscientiousness.

From independent component analysis of functional connectivity has emerged the perspective that spontaneous baseline activity of the brain is consistent across subjects (7). Prior work in functional connectivity has isolated canonical functional networks through independent component analysis on large group datasets (2-4, 10). PCA, or "eigenconnectivity" analyses, allow additional metrics of network stability and metastability to quantitative assessments of resting state functional connectivity (14).

Complex mental representations stand in contrast to cognition driven primarily by sensory input or external task constraints. As a category of cognition, self-generated thought is complex and heterogeneous. Understanding psychological and neural mechanisms underlying adaptive and maladaptive outcomes has been a key aim in recent years (125). Maladaptive outcomes of self-generated thought might include thoughts leading to distress and unhappiness that disrupt task performance. Adaptive outcomes of self-generated thought might include creative insight and problem-solving. A key component of social cognition is the ability to infer the thoughts and beliefs of other people, along with their feelings. These processing collectively are termed mentalizing (126). Mentalizing relies on self-generated thoughts, since humans do not have direct perceptual access to other people's thoughts. While certainly not the sole output for self-generated thought, social cognitive processes rely on numerous modalities of self-generated thinking, including concepts of personal identity,

mental inference of others' thoughts and feelings, and prediction. Therefore, healthy default mode network activity is essential in proper functioning of social cognitive abilities (127).

Considerable controversy and debate has centered on the utility of resting-state activity in cognitive neuroscience. Functional connectivity appears to play an active role in dynamic processes of cognition, not limited to passive or epiphenomenal activity, as some critics have contended (128-130). While literature into the correspondence of cognitive function with typicality in functional connectivity is limited, convincing evidence is accumulating to demonstrate departures from typical connectivity corresponding with pathology. For example, diosyncratic brain activation patterns predict impaired cognitive function in both autism (131, 132) and Down Syndrome (133).

Conscientiousness represents a core trait in personality psychology, along with extraversion, neuroticism, openness, and agreeableness (134). Conscientiousness is a marker of motivational stability, and as a trait corresponds to maintaining resistance to disruption and focus on ongoing goals The function of conscientiousness is posited as facilitating the pursuit of non-immediate goals and rule-based behavior (140). It is critical to resolve the underlying neurobiology of behavioral constructs in order to fully appreciate mechanistic differences and similarities giving rise to individual differences. The delayed convergence of individual subjects' functional architecture to final DMN steady-state activity provides a provocative positive finding for neural correspondence with conscientiousness in behavioral evaluation.

Although the Human Connectome Project represents a highly-powered study with robust single-subject connectivity measurements, limitations must be noted. The study is limited to healthy control adults. Behavioral and physiological data must be collected across the lifespan in order to track healthy development at all stages of the lifespan. Further, the dataset includes no information on clinical or nontypically developing populations and subpopulations. As such, it is limited in the amount of translational medical data can be derived from the Human Connectome Project at this point in time. A subset of the subjects are genetically related, which may bias conclusions toward overrepresented genotypes. Limitations in behavioral data itself include potential idiosyncratic behavior scores reflecting the metrics used in the battery, or the manner of data collection (e.g., observation of performance versus self-report measures). The findings may be variable to specific behavioral clustering schemes used. Simulated brain activity, while fruitful in elucidating functional connectivity biomarkers that correspond to behavioral observations, is simple and does not include sensory input, noise, or oscillations (135).

Despite limitations, the Human Connectome Project dataset allows a rigorous test of relationships between principal components of functional connectivity and behavior. Dynamical stability of the default mode network and typicality of principal components of functional connectivity appear related to sociality and higher-order cognitive performance in the Human Connectome Project dataset. These findings suggest the possibility of neural correlates of intelligence, prosociality, and conscientiousness in single subjects.

Methods

Resting State Functional Connectivity

Resting state functional connectivity was analyzed for 475 subjects from the Human Connectome Project. BOLD fMRI data was acquired in four 15-minute blocks per subject. FIX ICA cleaned data were used for analysis (113-119). The supratentorial cerebral cortex were parcellated into 333 regions as per Gordon et al. (136). Fourteen subject-specific subcortical regions were added using Freesurfer-derived segmentation (137) of bilateral thalamus, caudate, putamen, amygdala, hippocampus, pallidum, and nucleus accumbens. Fourteen cerebellar regions were added by using the parcellation of Buckner et al. (4) and using a 7-network parcellation split into left- and right-hemispheric regions. This parcellation scheme comprised a total of 361 regions, and a BOLD time series for each ROI was extracted and Fisher-transformed Pearson correlation coefficients were obtained for each pair of ROI's in each 15-minute block for each subject. The resulting 361 x 361 matrices were averaged across the four blocks for each subject, and averaged across all subjects to obtain a group-level functional connectivity matrix.

Principal components (eigennetworks) were identified using singular value decomposition of the 361 x 361 functional connectivity matrices. The first ten eigennetworks were calculated from the group mean connectivity matrix and back projected onto anatomical space (Figure 12A). The first 20 eigennetworks were identified in the same manner for each subject. Correlation coefficients across ROIs were computed between eigennetworks 1 through 20 for each

subject and eigennetworks one through ten from group mean connectivity. The ordinal ranking of single-subject eigennetworks best matched to each of the ten group-level eigennetworks were compiled to assess homogeneity of single-subject eigennetworks across the population (Figure 12B).

Behavioral Clusters

39 behavioral and psychometric assessments were selected from the Human Connectome Project behavioral dataset. Domains of behavior were selected based on theoretical relevance (e.g., grip strength was deemed irrelevant to this study) and avoidance of redundancy in psychometric features. The 39 behavioral domains were clustered using principal component analysis across 475 subjects, with orthogonal rotation of components. Behavioral measurements organized into ten components which, based on loading factors of individual measures, were identified as relevant to 1) social support, 2) negative affect, 3) intelligence, 4) executive function, 5) delay discounting, 6) positive affect, 7) memory, 8) prosociality, 9) conscientiousness, and 10) attention (Figure 13). An individual subject's score for a behavioral cluster was a weighted average of their normalized scores on the individual metrics shown in Figure 13.

Behavior/Connectivity Correlation

To assess significant covariations across behavioral and RSFC data, single-subjects' eigennetworks were ordered to correspond with the eigennetwork of greatest homology by spatial correlation coefficient across ROIs.

In this reordered paradigm, Spearman correlation coefficient was calculated between eigenvalues for single-subject networks and individuals' scores for the ten behavioral clusters. Because of the clear correspondence of group-level eigennetwork 2 with canonical default mode network architecture, we also investigated correlations across behavioral factors and default mode network (group-level eigennetwork 2) variations. Spearman correlations were calculated between eigennetwork 2 for each individual subject and eigennetwork 2 from group mean data. Using these subject-to-group correlation scores for eigennetwork 2 (similarity to the group mean), Spearman correlation was then calculated between these values and the behavioral cluster scores across subjects. Statistical significance was assessed in all cases using acceptable false discovery rate $q<0.05$.

Dynamical Simulations

In order to simulate evolution of whole brain network activity over time, we modeled brain activity over time as previously described (94). Briefly, we began with activity in a single brain region by constructing a vector with 361 elements and assigning a region to 1 and all other regions to 0. In a stepwise process, the vector was multiplied by the functional connectivity matrix, and the result was then normalized by subtracting the mean and dividing by the standard deviation across regions. This was repeated for 40 temporal "steps", and performed using each of the 361 ROIs as a starting region in each subject and for the group mean functional connectivity. Convergence was determined by the mean absolute

difference in stepwise vectors to within a tolerance of less than 0.05% change in the mean absolute intensity value across the ROIs.

To assess the predictive value of simulation parameters and behavior, Spearman correlation coefficients were calculated between each of the ten behavioral cluster scores and three simulation parameters; namely, similarity between single-subject convergence states and mean group-level convergence state; total number of local minima in each subjects' simulations; and minimum number of convergence steps.

CHAPTER 5

CONCLUSIONS

I entered the bioengineering program at the University of Utah with enthusiasm, and am happy to convey that I am just as, if not more, enthusiastic as ever about the present and the future of Homo sapiens' ability to understand, describe, and intervene in the systems of their own biology. We are a richly creative species, with problem solving abilities to address challenges of suffering on a depth and scale unimaginable in many ways until even a few decades ago.

Advances in brain imaging technologies affect, and will continue to affect, society beyond the research laboratory and the clinic. A rapidly growing series of applications from biomedical imaging are being seen, for example, in the court system. Aggressive attempts are being made to design and implement sophisticated lie detection techniques to surpass the sensitivity and specificity of the current polygraph test. The ramifications of this single bioengineering accomplishment stimulate the imagination as one considers the impact that next generation lie detection will have on the evidence used in criminal and civil cases, law enforcement, and security in corporate and government operations. Under a different area of neuroscience and law, efforts are underway to use advanced methods of brain imaging to assess traumatic brain injury sustained by

workplace accident or occupational hazard; war and military service; negligence; or any other number of claims for personal injury.

A primary take-home message is that through the functional connectome, especially that collected through RSFC, we have a mathematical representation of sophisticated whole brain processes. These processes represent contributions to behavior and cognition at the individual level. We are quickly approaching an era of personalized neuroscience, wherein longitudinal tracking of RSFC profiles in a single subject across the lifespan may be a medical reality of standard care, in addition to a scientific fact of large-group study samples. Because the data-rich architecture of RSFC will continue to provide key features through biomarkers developed for understanding cognition and disease, we only expect RSFC profiles to become more ubiquitous in their use and commonplace in their acquisition. Health privacy measures must be strictly maintained in the new era of personalized neuroscience, as they are for any other personally identifying and consequential data, such as a person's genome.

Functional connectivity MRI (fcMRI) and resting state functional connectivity (RSFC) in particular are widely used for measuring correlation of activity between cortical regions, and it is a rapidly expanding tool of choice to examine basic science, medical, and philosophical questions. Resources invested into directed science and technology development from federal initiatives such as the Human Connectome Project and the Brain Initiative help reinforce growth of methods and applications in cutting edge neuroscience and cognitive science. Industry opportunities continue to arise in applications of fcMRI

to pharmacological development for undertreated and mistreated clinical conditions, as do opportunities to track myriad interventions and their impact longitudinally on brain and mind, as in the speed reading example in this text.

I have demonstrated that simulations of whole brain activity presently available for population level and individual difference analysis are able to present biomarkers for behavior from neurophysiological features previously unnoted. By using weighted connection strengths between regions to iterate brain activity in discrete steps, we identified metastable intermediate states in our simulation that correspond to combinations of functional networks previously characterized through ICA of RSFC. Convergence to a final state was slowest for initial conditions on the borders of the default mode network, and future work to develop mathematical simulations of whole brain activity will explore how hubs of activity act as attractors through systems methods. The strongest attractor in the simulation is the default mode network, with reliable, consistent, reproducible convergence to DMN configuration at the final stability point for simulated activity. This method is reproducible at a single-subject level of analysis, and is sensitive to changes in functional connectivity affected by task-specific dynamics. Future work will continue to demonstrate and elaborate on metastable qualities of the human connectome.

To study neuroplasticity and use the tools of functional connectivity in a longitudinal study, we examined the impact of a short-term speed reading program on a small cohort of adolescents. A goal of interventions designed to increase reading speed is to reduce the practice of articulating words in an

individual's thoughts, or subvocalization. Reading is a complex behavior involving numerous overlapping networks in the brain for high-level information synthesis. For most people, reading draws on redundant cognitive resources that slow reading speed, and detract from efficient semantic understanding. We found significantly decreased correlation between left Broca Area and right Broca Homologue and between right Broca Homologue and right Wernicke Homologue in the resting state after the training period compared to before training in which participants were trained to eliminate subvocalization or words from their reading style. Differences in functional connectivity after training to left Broca Area showed a spatial distribution reflecting decreased correlation to memory-associated brain regions and increased correlation to auditory regions, which might be consistent with a hypothesis that such training may decrease subvocalization associated with semantic memory function during the resting state.

In the final study published in this dissertation, we examine the relationship of RSFC with behavior more closely. Using principal component analysis to decompose resting-state functional connectivity matrices, we examined principal components (eigennetworks) with the largest eigenvalues, comprising the greatest variance of group- and single-subject level functional connectivity. Behavioral data from the 475 study participants clustered into ten categories of behavioral features: social support, negative affect, intelligence, executive function, delay discounting, positive affect, memory, prosociality, conscientiousness, and attention. Domains of conscientiousness, prosociality,

and intelligence were determined to significantly relate at the individual subject level to patterns of RSFC identified through eigenanlysis and simulation of whole brain activity.

Cognitive performance (intelligence) across 475 subjects is significantly correlated with the eigenvalue of four of the ten eigennetworks, indicating that the degree to which highest-ordered group-level components are present in the subject's principal components reflect cognitive performance on behavioral tasks. Conscientiousness in individual behavior is inversely predicted by how quickly individual subjects' simulated brains converge to steady-state default mode network architecture. In other words, the longer it takes a subjects' brain to converge to a final default mode network steady-state, the higher the individual scores on behavioral measures of conscientiousness. Conscientiousness represents a core trait in personality psychology, along with extraversion, neuroticism, openness, and agreeableness (134). Conscientiousness is a marker of motivational stability, and as a trait corresponds to maintaining resistance to disruption and focus on ongoing goals. The function of conscientiousness is posited as facilitating the pursuit of nonimmediate goals and rule-based behavior. It is critical to resolve the underlying neurobiology of behavioral constructs in order to fully appreciate mechanistic differences and similarities giving rise to individual differences. The delayed convergence of individual subjects' functional architecture to final DMN steady-state activity provides a provocative positive finding for neural correspondence with conscientiousness in behavioral evaluation.

Prosociality across individuals is significantly correlated with the closeness of fit between individuals' EN2 and group-mean EN2. Because group-mean EN2 represents the default mode network identified in traditional ICA of RSFC, we assert that prosociality in a healthy control population is predicted by the typicality of an individuals' default mode network, or similarity of the network to the group-averaged default mode network. It is notable that prosociality is not predicted by strength of DMN activity reflected in EN2's eigenvalue. Only the coherence to group-mean architecture and not variations in EN2's weighted contribution to functional connectivity predicted prosocial behavior. Simulated dynamic activity of individual subjects' brains reveals functional markers for conscientiousness.

Because prosociality is significantly linked to healthy default mode network architecture, it becomes important to understand the broader function of the DMN in cognition if one is to appreciate the elemental cognitive processes that support prosocial behavior. Self-generated, complex thought is in contract to cognition driven by sensory input or external task constraints. It aligns elegantly with cognitive theory to see a mathematical description of resting state brain activity in which the primary mode driving whole brain action is the primary sensory and visual cortex (eigennetwork 1 in group-mean HCP500). The second greatest contribution to resting state brain activity comes from the default mode network, as demonstrated by group-mean eigennetwork 2 in the Human Connectome Project 500 dataset. Social cognitive processes rely on numerous modalities of self-generated thinking including concepts of personal identity, mental inference

of others' thoughts and feelings, and prediction. Therefore, healthy default mode network activity is essential in proper functioning of social cognitive abilities (127). Limitations previously noted in the Human Connectome Project dataset could be reframed as signal of opportunity. While the HCP study is limited to healthy control adults, collection of comparable large sample or multisite clinical RSFC profiles will immediately yield insight into the nature of a multitude of disease states. Although behavioral data were useful in finding positive associations between brain and behavior, much more behavioral information must be spanned in future large-scale efforts to map the interface of behavior and brain. Several of such efforts are underway at Harvard University, Cornell University, and other private institutions, along with data-sharing initiatives that are actively assembling clinically-relevant repositories of behavioral and imaging data.

REFERENCES

1. Ferguson MA, Nielsen JA, & Anderson JS (2014) Altered resting functional connectivity of expressive language regions after speed reading training. *J Clin Exp Neuropsychol* (ahead-of-print):1-12.

2. Biswal BB*, et al.* (2010) Toward discovery science of human brain function. *Proc Natl Acad Sci U S A* 107(10):4734-4739.

3. Fox MD & Raichle ME (2007) Spontaneous fluctuations in brain activity observed with functional magnetic resonance imaging. *Nat Rev Neurosci* 8(9):700-711.

4. Yeo BT*, et al.* (2011) The organization of the human cerebral cortex estimated by intrinsic functional connectivity. *J Neurophys* 106(3):1125-1165.

5. Biswal B, Yetkin FZ, Haughton VM, & Hyde JS (1995) Functional connectivity in the motor cortex of resting human brain using echo-planar MRI. *Magn Reson Med* 34(4):537-541.

6. Raichle ME*, et al.* (2001) A default mode of brain function. *Proc Natl Acad Sci U S A* 98(2):676-682.

7. Damoiseaux JS*, et al.* (2006) Consistent resting-state networks across healthy subjects. *Proc Natl Acad Sci U S A* 103(37):13848-13853.

8. Jafri MJ, Pearlson GD, Stevens M, & Calhoun VD (2008) A method for functional network connectivity among spatially independent resting-state components in schizophrenia. *Neuroimage* 39(4):1666-1681.

9. Beckmann CF & Smith SM (2004) Probabilistic independent component analysis for functional magnetic resonance imaging. *IEEE Trans Med Imaging* 23(2):137-152.

10. Power JD*, et al.* (2011) Functional network organization of the human brain. *Neuron* 72(4):665-678.

11. Honey CJ*, et al.* (2009) Predicting human resting-state functional connectivity from structural connectivity. *Proc Natl Acad Sci U S A* 106(6):2035-2040.
12. Smith SM*, et al.* (2009) Correspondence of the brain's functional architecture during activation and rest. *Proc Natl Acad Sci U S A* 106(31):13040-13045.

13. Van Dijk KR*, et al.* (2010) Intrinsic functional connectivity as a tool for human connectomics: theory, properties, and optimization. *J Neurophysiol* 103(1):297-321.

14. Leonardi N*, et al.* (2013) Principal components of functional connectivity: a new approach to study dynamic brain connectivity during rest. *Neuroimage* 83:937-950.

15. Smith SM*, et al.* (2011) Network modelling methods for FMRI. *Neuroimage* 54(2):875-891.

16. Just MA, Cherkassky VL, Keller TA, & Minshew NJ (2004) Cortical activation and synchronization during sentence comprehension in high-functioning autism: evidence of underconnectivity. *Brain* 127(Pt 8):1811-1821.

17. Greicius MD, Srivastava G, Reiss AL, & Menon V (2004) Default-mode network activity distinguishes Alzheimer's disease from healthy aging: evidence from functional MRI. *Proc Natl Acad Sci U S A* 101(13):4637-4642.

18. Anderson JS*, et al.* (2011) Functional connectivity magnetic resonance imaging classification of autism. *Brain* 134(Pt 12):3742-3754.

19. Nielsen JA*, et al.* (2013) Multisite functional ocnnectivity MRI classification of autism: ABIDE results. *Front Hum Neurosci* 7:599.

20. Kapur S, Phillips AG, & Insel TR (2012) Why has it taken so long for biological psychiatry to develop clinical tests and what to do about it? *Mol Psychiatry* 17(12):1174-1179.

21. Ferguson MA & Anderson JS (2012) Dynamical stability of intrinsic connectivity networks. *Neuroimage* 59(4):4022-4031.

22. Altamirano F*, et al.* (2012) Increased resting intracellular calcium modulates NF-kappaB-dependent inducible nitric-oxide synthase gene expression in dystrophic mdx skeletal myotubes. *J Biol Chem* 287(25):20876-20887.

23. Hutchison RM*, et al.* (2013) Dynamic functional connectivity: promise, issues, and interpretations. *Neuroimage* 80:360-378.

24. Smith SL, Pichora-Fuller MK, Wilson RH, & Macdonald EN (2012) Word recognition for temporally and spectrally distorted materials: the effects of age and hearing loss. *Ear Hear* 33(3):349-366.

25. Leonardi N, Shirer WR, Greicius MD, & Van De Ville D (2014) Disentangling dynamic networks: Separated and joint expressions of functional connectivity patterns in time. *Hum Brain Mapp* 35(12):5984-5995.

26. Van Essen DC*, et al.* (2012) The Human Connectome Project: a data acquisition perspective. *NeuroImage* 62(4):2222-2231.

27. Anderson JS, Ferguson MA, Lopez-Larson M, & Yurgelun-Todd D (2011) Reproducibility of Functional Connectivity Measurements in Single Subjects. *AJNR Am J Neuroradiol* 32:548-555.

28. Shehzad Z*, et al.* (2009) The resting brain: unconstrained yet reliable. *Cereb Cortex* 19(10):2209-2229.

29. Birn RM*, et al.* (2013) The effect of scan length on the reliability of resting-state fMRI connectivity estimates. *Neuroimage* 83:550-558.

30. Power JD, Barnes KA, Snyder AZ, Schlaggar BL, & Petersen SE (2012) Spurious but systematic correlations in functional connectivity MRI networks arise from subject motion. *Neuroimage* 59(3):2142-2154.

31. Alter O (2007) Genomic signal processing: from matrix algebra to genetic networks. *Methods Mol Biol* 377:17-60.

32. Adelstein JS*, et al.* (2011) Personality is reflected in the brain's intrinsic functional architecture. *PLoS One* 6(11):e27633.

33. Kennis M, Rademaker AR, & Geuze E (2013) Neural correlates of personality: an integrative review. *Neurosci Biobehav Rev* 37(1):73-95.

34. Marcus DS*, et al.* (2011) Informatics and data mining tools and strategies for the human connectome project. *Front Neuroinform* 5:4.

35. Zhang D & Raichle ME (2010) Disease and the brain's dark energy. *Nat Rev Neurol* 6(1):15-28.

36. Fox MD*, et al.* (2005) The human brain is intrinsically organized into dynamic, anticorrelated functional networks. *Proc Natl Acad Sci U S A* 102(27):9673-9678.

37. Fransson P (2005) Spontaneous low-frequency BOLD signal fluctuations: an fMRI investigation of the resting-state default mode of brain function hypothesis. *Hum Brain Mapp* 26(1):15-29.

38. Fox MD, Zhang D, Snyder AZ, & Raichle ME (2009) The global signal and observed anticorrelated resting state brain networks. *J Neurophysiol* 101(6):3270-3283.

39. Murphy K, Birn RM, Handwerker DA, Jones TB, & Bandettini PA (2009) The impact of global signal regression on resting state correlations: are anti-correlated networks introduced? *Neuroimage* 44(3):893-905.

40. Anderson JS*, et al.* (2011) Network anticorrelations, global regression, and phase-shifted soft tissue correction. *Hum Brain Mapp* 32(6):919-934.

41. Kiviniemi V*, et al.* (2009) Functional segmentation of the brain cortex using high model order group PICA. *Hum Brain Mapp* 30(12):3865-3886.

42. Tomasi D & Volkow ND (2011) Association between Functional Connectivity Hubs and Brain Networks. *Cereb Cortex*.

43. Lowe MJ, Mock BJ, & Sorenson JA (1998) Functional connectivity in single and multislice echoplanar imaging using resting-state fluctuations. *Neuroimage* 7(2):119-132.

44. Cordes D*, et al.* (2000) Mapping functionally related regions of brain with functional connectivity MR imaging. *AJNR Am J Neuroradiol* 21(9):1636-1644.

45. Greicius MD, Krasnow B, Reiss AL, & Menon V (2003) Functional connectivity in the resting brain: a network analysis of the default mode hypothesis. *Proc Natl Acad Sci U S A* 100(1):253-258.

46. He Y*, et al.* (2009) Uncovering intrinsic modular organization of spontaneous brain activity in humans. *PLoS One* 4(4):e5226.

47. Raichle ME & Snyder AZ (2007) A default mode of brain function: a brief history of an evolving idea. *Neuroimage* 37(4):1083-1090; discussion 1097-1089.

48. Gusnard DA & Raichle ME (2001) Searching for a baseline: functional imaging and the resting human brain. *Nat Rev Neurosci* 2(10):685-694.

49. Gusnard DA, Akbudak E, Shulman GL, & Raichle ME (2001) Medial prefrontal cortex and self-referential mental activity: relation to a default mode of brain function. *Proc Natl Acad Sci U S A* 98(7):4259-4264.

50. Northoff G*, et al.* (2006) Self-referential processing in our brain--a meta-analysis of imaging studies on the self. *Neuroimage* 31(1):440-457.

51. Cavanna AE & Trimble MR (2006) The precuneus: a review of its functional anatomy and behavioural correlates. *Brain* 129(Pt 3):564-583.

52. Deco G, Jirsa VK, & McIntosh AR (2010) Emerging concepts for the dynamical organization of resting-state activity in the brain. *Nat Rev Neurosci* 12(1):43-56.

53. Honey CJ, Kotter R, Breakspear M, & Sporns O (2007) Network structure of cerebral cortex shapes functional connectivity on multiple time scales. *Proc Natl Acad Sci U S A* 104(24):10240-10245.

54. Ghosh A, Rho Y, McIntosh AR, Kotter R, & Jirsa VK (2008) Noise during rest enables the exploration of the brain's dynamic repertoire. *PLoS Comput Biol* 4(10):e1000196.

55. Deco G, Jirsa V, McIntosh AR, Sporns O, & Kotter R (2009) Key role of coupling, delay, and noise in resting brain fluctuations. *Proc Natl Acad Sci U S A* 106(25):10302-10307.

56. Anderson JS, Ferguson MA, Lopez-Larson M, & Yurgelun-Todd D (2011) Reproducibility of single-subject functional connectivity measurements. *AJNR Am J Neuroradiol* 32(3):548-555.

57. Anderson JS, Ferguson MA, Lopez-Larson M, & Yurgelun-Todd D (2010) Topographic maps of multisensory attention. *Proc Natl Acad Sci U S A* 107(46):20110-20114.

58. Sun FT, Miller LM, & D'Esposito M (2004) Measuring interregional functional connectivity using coherence and partial coherence analyses of fMRI data. *Neuroimage* 21(2):647-658.

59. Salvador R*, et al.* (2007) Frequency based mutual information measures between clusters of brain regions in functional magnetic resonance imaging. *Neuroimage* 35(1):83-88.

60. Marrelec G*, et al.* (2006) Partial correlation for functional brain interactivity investigation in functional MRI. *Neuroimage* 32(1):228-237.

61. Trefethen LN & Bau III D (1997) *Numerical Linear Algebra* (SIAM: Society for Industrial and Applied Mathematics, Philadelphia).

62. Anderson JS (2008) Origin of synchronized low-frequency blood oxygen level-dependent fluctuations in the primary visual cortex. *AJNR Am J Neuroradiol* 29(9):1722-1729.

63. Cordes D*, et al.* (2001) Frequencies contributing to functional connectivity in the cerebral cortex in "resting-state" data. *AJNR Am J Neuroradiol* 22(7):1326-1333.

64. Little MA, McSharry PE, Roberts SJ, Costello DA, & Moroz IM (2007) Exploiting nonlinear recurrence and fractal scaling properties for voice disorder detection. *Biomed Eng Online* 6:23.

65. Anderson JS*, et al.* (2011) Functional Connectivity MRI Classification of Autism. *Brain* In Press.

66. Anderson JS, Ferguson MA, Lopez-Larson M, & Yurgelun-Todd D (2011) Connectivity Gradients Between the Default Mode and Attention Control Networks. *Brain Conn* 1(2):147-157.

67. Buckner RL*, et al.* (2009) Cortical hubs revealed by intrinsic functional connectivity: mapping, assessment of stability, and relation to Alzheimer's disease. *J Neurosci* 29(6):1860-1873.

68. Cole MW, Pathak S, & Schneider W (2009) Identifying the brain's most globally connected regions. *Neuroimage* 49(4):3132-3148.

69. Hagmann P*, et al.* (2008) Mapping the structural core of human cerebral cortex. *PLoS Biol* 6(7):e159.

70. Cohen AL*, et al.* (2008) Defining functional areas in individual human brains using resting functional connectivity MRI. *Neuroimage* 41(1):45-57.

71. Sporns O, Chialvo DR, Kaiser M, & Hilgetag CC (2004) Organization, development and function of complex brain networks. *Trends Cogn Sci* 8(9):418-425.

72. Dosenbach NU*, et al.* (2010) Prediction of individual brain maturity using fMRI. *Science* 329(5997):1358-1361.

73. Fair DA*, et al.* (2008) The maturing architecture of the brain's default network. *Proc Natl Acad Sci U S A* 105(10):4028-4032.

74. Reynolds JH & Heeger DJ (2009) The normalization model of attention. *Neuron* 61(2):168-185.

75. Calhoun VD, Maciejewski PK, Pearlson GD, & Kiehl KA (2008) Temporal lobe and "default" hemodynamic brain modes discriminate between schizophrenia and bipolar disorder. *Hum Brain Mapp* 29(11):1265-1275.

76. Rombouts SA*, et al.* (2009) Model-free group analysis shows altered BOLD FMRI networks in dementia. *Hum Brain Mapp* 30:256-266.

77. Liu YY, Slotine JJ, & Barabasi AL (2011) Controllability of complex networks. *Nature* 473(7346):167-173.

78. Fransson P (2006) How default is the default mode of brain function? Further evidence from intrinsic BOLD signal fluctuations. *Neuropsychologia* 44(14):2836-2845.

79. Schlaggar BL & McCandliss BD (2007) Development of neural systems for reading. *Annu Rev Neurosci* 30:475-503.

80. Posner MI, Petersen SE, Fox PT, & Raichle ME (1988) Localization of cognitive operations in the human brain. *Science* 240(4859):1627-1631.

81. Share DL (1995) Phonological recoding and self-teaching: sine qua non of reading acquisition. *Cognition* 55(2):151-218; discussion 219-126.

82. Raij T, Uutela K, & Hari R (2000) Audiovisual integration of letters in the human brain. *Neuron* 28(2):617-625.

83. Pugh KR*, et al.* (2001) Neurobiological studies of reading and reading disability. *J Commun Disord* 34(6):479-492.

84. van Atteveldt N, Formisano E, Goebel R, & Blomert L (2004) Integration of letters and speech sounds in the human brain. *Neuron* 43(2):271-282.

85. Temple E*, et al.* (2003) Neural deficits in children with dyslexia ameliorated by behavioral remediation: evidence from functional MRI. *Proc Natl Acad Sci U S A* 100(5):2860-2865.

86. Aylward EH*, et al.* (2003) Instructional treatment associated with changes in brain activation in children with dyslexia. *Neurology* 61(2):212-219.

87. Kujala T*, et al.* (2001) Plastic neural changes and reading improvement caused by audiovisual training in reading-impaired children. *Proc Natl Acad Sci U S A* 98(18):10509-10514.

88. Simos PG*, et al.* (2002) Dyslexia-specific brain activation profile becomes normal following successful remedial training. *Neurology* 58(8):1203-1213.

89. Shaywitz BA*, et al.* (2004) Development of left occipitotemporal systems for skilled reading in children after a phonologically- based intervention. *Biol Psychiatry* 55(9):926-933.

90. Bosshardt HG (1990) Subvocalization and reading rate differences between stuttering and nonstuttering children and adults. *J Speech Hear Res* 33(4):776-785.

91. Wiederholt J & Bryant B (2001) *Gray oral reading tests- (GORT-4).* (Pro-Ed, Austin).

92. Anderson JS*, et al.* (2010) Decreased Left Posterior Insular Activity During Auditory Langauge in Autism. *AJNR. Am J Neuroradiol* 31:131-139.

93. Anderson JS*, et al.* (2011) Functional connectivity magnetic resonance imaging classification of autism. *Brain* 134(12):3742-3754.

94. Ferguson MA & Anderson JS (2011) Dynamical stability of intrinsic connectivity networks. *Neuroimage* 59(4):4022-4031.

95. Yarkoni T, Poldrack RA, Nichols TE, Van Essen DC, & Wager TD (2011) Large-scale automated synthesis of human functional neuroimaging data. *Nat Methods* 8(8):665-670.

96. Bullmore ET*, et al.* (1996) Functional magnetic resonance image analysis of a large-scale neurocognitive network. *NeuroImage* 4(1):16-33.

97. Hinke RM*, et al.* (1993) Functional magnetic resonance imaging of Broca's area during internal speech. *Neuroreport* 4(6):675-678.

98. McFarland MJ, Watkins JW, Kordich MM, Pollet DA, & Palmer GR (2004) Use of noise attenuation modeling in managing missile motor detonation activities. *J Air Waste Manag Assoc* 54(3):342-351.

99. Dien J & O'Hare AJ (2008) Evidence for automatic sentence priming in the fusiform semantic area: convergent ERP and fMRI findings. *Brain Res* 1243:134-145.

100. Finney EM, Clementz BA, Hickok G, & Dobkins KR (2003) Visual stimuli activate auditory cortex in deaf subjects: evidence from MEG. *Neuroreport* 14(11):1425-1427.

101. Morel L*, et al.* (2008) [A new treatment: bariatric surgery; a new complication: Wernicke-Korsakoff encephalopathy]. *Presse Med* 37(1 Pt 1):49-53.

102. Price CJ (2010) The anatomy of language: a review of 100 fMRI studies published in 2009. *Ann N Y Acad Sci* 1191:62-88.

103. Perani D*, et al.* (2011) Neural language networks at birth. *Proc Natl Acad Sci U S A* 108(38):16056-16061.

104. David O, Maess B, Eckstein K, & Friederici AD (2011) Dynamic causal modeling of subcortical connectivity of language. *J Neurosci* 31(7):2712-2717.

105. Cai Q, Paulignan Y, Brysbaert M, Ibarrola D, & Nazir TA (2010) The left ventral occipito-temporal response to words depends on language lateralization but not on visual familiarity. *Cereb Cortex* 20(5):1153-1163.

106. Hellyer PJ, Woodhead ZV, Leech R, & Wise RJ (2011) An investigation of twenty/20 vision in reading. *J Neurosci* 31(41):14631-14638.

107. Guo X*, et al.* (2011) Acquisition of conscious and unconscious knowledge of semantic prosody. *Conscious Cogn* 20(2):417-425.

108. Borowsky R, Esopenko C, Cummine J, & Sarty GE (2007) Neural representations of visual words and objects: a functional MRI study on the modularity of reading and object processing. *Brain Topogr* 20(2):89-96.

109. Binder JR, Desai RH, Graves WW, & Conant LL (2009) Where is the semantic system? A critical review and meta-analysis of 120 functional neuroimaging studies. *Cereb Cortex* 19(12):2767-2796.

110. Price SE*, et al.* (2012) Semantic verbal fluency strategies in amnestic mild cognitive impairment. *Neuropsychology* 26(4):490-497.

111. Xiang HD, Fonteijn HM, Norris DG, & Hagoort P (2010) Topographical functional connectivity pattern in the perisylvian language networks. *Cereb Cortex* 20(3):549-560.

112. Yeo BT*, et al.* (2014) Functional Specialization and Flexibility in Human Association Cortex. *Cereb Cortex*.

113. Feinberg DA*, et al.* (2010) Multiplexed echo planar imaging for sub-second whole brain FMRI and fast diffusion imaging. *PLoS One* 5(12):e15710.

114. Glasser MF*, et al.* (2013) The minimal preprocessing pipelines for the Human Connectome Project. *Neuroimage* 80:105-124.

115. Moeller S*, et al.* (2010) Multiband multislice GE-EPI at 7 tesla, with 16-fold acceleration using partial parallel imaging with application to high spatial and temporal whole-brain fMRI. *Magn Reson Med* 63(5):1144-1153.

116. Setsompop K*, et al.* (2012) Blipped-controlled aliasing in parallel imaging for simultaneous multislice echo planar imaging with reduced g-factor penalty. *Magn Reson Med* 67(5):1210-1224.

117. Van Essen DC*, et al.* (2013) The WU-Minn Human Connectome Project: an overview. *Neuroimage* 80:62-79.

118. Xu J*, et al.* (2012) Highly Accelerated Whole Brain Imaging Using Aligned-Blipped-Controlled-aliasing Multiband EPI. *Proc. Int. Soc. Mag. Reson. Med* 20:2306.

119. Griffanti L*, et al.* (2014) ICA-based artefact removal and accelerated fMRI acquisition for improved resting state network imaging. *Neuroimage* 95:232-247.

120. Smith S*, et al.* (2015) HCP beta-release of the Functional Connectivity MegaTrawl.

121. Smith SM*, et al.* (2013) Resting-state fMRI in the Human Connectome Project. *NeuroImage* 80:144-168.

122. Smith SM, Hyvarinen A, Varoquaux G, Miller KL, & Beckmann CF (2014) Group-PCA for very large fMRI datasets. *Neuroimage* 101:738-749.

123. Moore BC (1981) Principal component analysis in linear systems: Controllability, observability, and model reduction. *IEEE Trans Automatic Control* 26(1):17-32.

124. Mars RB*, et al.* (2012) On the relationship between the "default mode network" and the "social brain". *Front Hum Neurosci* 6:189.

125. Andrews-Hanna JR, Smallwood J, & Spreng RN (2014) The default network and self-generated thought: component processes, dynamic control, and clinical relevance. *Ann N Y Acad Sci* 1316:29-52.

126. Frith U & Frith CD (2003) Development and neurophysiology of mentalizing. *Philosophical Transactions of the Royal Society of London. Series B, Biological Sciences* 358(1431):459-473.

127. Spunt RP, Meyer ML, & Lieberman MD (2015) The default mode of human brain function primes the intentional stance. *J Cogn Neurosci* 27(6):1116-1124.

128. Spreng RN*, et al.* (2014) Goal-congruent default network activity facilitates cognitive control. *J Neurosci* 34(42):14108-14114.

129. Spreng RN, Gerlach KD, Turner GR, & Schacter DL (2015) Autobiographical Planning and the Brain: Activation and Its Modulation by Qualitative Features. *J Cogn Neurosci*:1-11.

130. Spreng RN & Schacter DL (2012) Default network modulation and large-scale network interactivity in healthy young and old adults. *Cereb Cortex* 22(11):2610-2621.

131. Byrge L, Dubois J, Tyszka JM, Adolphs R, & Kennedy DP (2015) Idiosyncratic brain activation patterns are associated with poor social comprehension in autism. *J Neurosci* 35(14):5837-5850.

132. Hahamy A, Behrmann M, & Malach R (2015) The idiosyncratic brain: distortion of spontaneous connectivity patterns in autism spectrum disorder. *Nat Neurosci*.

133. Anderson JS*, et al.* (2013) Abnormal Brain Synchrony in Down Syndrome. *NeuroImage: Clinical* 2:703-715.

134. Costa PT & McCrae RR (2008) The revised neo personality inventory (neo-pi-r). *The SAGE Handbook of Personality Theory and Assessment* 2:179-198.

135. Hansen EC, Battaglia D, Spiegler A, Deco G, & Jirsa VK (2015) Functional connectivity dynamics: modeling the switching behavior of the resting state. *Neuroimage* 105:525-535.

136. Gordon EM*, et al.* (2014) Generation and Evaluation of a Cortical Area Parcellation from Resting-State Correlations. *Cereb Cortex*.

137. Fischl B*, et al.* (2002) Whole brain segmentation: automated labeling of neuroanatomical structures in the human brain. *Neuron* 33(3):341-355.